Manufacturing and Characterization of Epoxy Based Flexible Thermoelectric Modules

Quanzeng Zhang

School of Science

Thesis submitted for examination for the degree of Master of Science in Technology.
Espoo 23.3.2023

Supervisor

>Prof. Sillanpää Mika

Advisors

>Anurak Sawatdee MSc

>Prof. Zia Ullah Khan

Aalto University
School of Science

Author Quanzeng Zhang	
Title Manufacturing and Characterization of Epoxy Based Flexible Thermoelectric Modules	
Degree programme Engineering Physics	
Major Advanced Energy Technology	**Code of major**
Supervisor Prof. Sillanpää Mika	
Advisors Anurak Sawatdee MSc, Prof. Zia Ullah Khan	
Date 23.3.2023 **Number of pages** 41+4	**Language** English

Abstract

Thermoelectric module can convert waste heat into electricity due to its unique Seebeck effect. Since a great deal of heat produced in households and factories has been wasted. It is significant to collect the waste heat by thermoelectric modules. However, conventional thermoelectric modules mainly possess rigid substrates, which limits their applications in complex situations, such as the industrial pipe and human body. Thermoelectric modules with flexible substrates can overcome this drawback. Flexible thermoelectric module can be bent to adapt to uneven surfaces. Hence, it requires superior mechanical strength in order not to break when bent. The mechanical strength highly relies on the binding material. Binding materials can be classified into solder paste and electrically conductive adhesive. This work presents a new electrically conductive adhesive named 2D-ECA, synthesized by RISE (Research Institutes of Sweden) and Linköping University. Various characterization methods have been applied to study its performance in the device.

In this work, we mainly focused on the mechanical strength, electric conductivity and thermoelectric property of 2D-ECA. We found that the mechanical strength of 2D-ECA is as high as superior commercial solder paste and electrically conductive adhesive. What's more, 2D-ECA will not damage the inherent mechanical strength of the thermoelectric leg as the solder paste. However, the electric resistance of 2D-ECA based samples is considerably higher than solder pastes. As a result, devices fabricated with 2D-ECA showed a relatively lower output power. Hence, further research should focus on improving the electrical conductivity of 2D-ECA. Nevertheless, further study illustrated that 2D-ECA can be used on aluminium substrate, while it is impossible for ordinary solder pastes. It is a significant step towards low-cost devices.

Keywords Flexible thermoelectric module, 2D-ECA, Mechanical strength, Output power

Preface

I want to thank Anurak Sawatdee, professor Zia and Mika for their guidance in this master's thesis work. Ek is both a careful advisor and a funny friend to me. He taught me how to do good research work independently, which is a priceless wealth for me to carry on as a researcher. I also got a lot of help in daily life from him, it made me feel at home when working at RISE. I really appreciated it. Zia gave me much advice on the experiment work, which is wise and forward-looking. Working in the clean room is also a special experience for me, thanks to Zia's guidance. Mika did a lot of work on the master's thesis as a supervisor, I am really grateful for his continuous effort in the whole process. I also want to thank all my colleagues at RISE, they offered me a lot of help while working at RISE. Especially Jan, Olle and Mohammad from ParsNord, helped me a lot with research and equipment, and I learnt a lot from them.

I also want to thank my family and friends at Aalto. I have had a happy school life with their full support. These beautiful memories will be eternal in my life.

Otaniemi, 20/3/2023

Quanzeng Zhang

Contents

Symbols and abbreviations

Symbols

S	Seebeck coefficient
Π	Peltier coefficient
N_a	Avogadro constant

Abbreviations

TEM	Thermoelectric module
FTEM	Flexible thermoelectric module
ECA	Electrical conductive adhesive
PET	Polyethylene terephthalate
PI	Polyimide

1 Introduction

Energy has been extremely important in human life since tens of thousands of years ago. However, the energy resource limitation problem becomes severe now. Due to the overexploitation of non-renewable energy resources (such as coal, oil, and natural gas), the proven reserves may be depleted within 200 years [1]. Despite the increasingly serious energy problems, various energy resources including solar, wind, hydro energy, and waste heat have not been used efficiently. Especially waste heat, a great amount of energy consumed in factories and households is lost to the environment in the form of heat without any retrieval.

Thermoelectric energy conversion is a promising method to reclaim waste heat. Based on the Seebeck effect, thermoelectric devices can convert thermal energy to electricity. With the development of efficient thermoelectric materials, thermoelectric modules have been put into commercial use known as the Peltier element. Owing to the advantages of silent, no moving part, reliable, and small in size, thermoelectric modules (TEMs) have been widely used in the fields related to electronics, medicine, industry, and consumer technology. For example, TEMs are particularly suited for wearable devices such as medical sensors, smart watches, smart clothes and shoes, and earphones. It is not only because they can generate electricity from human body to power the devices, but also because they are silent, small, and extremely stable, which means there is no need to maintain them like traditional batteries. Waste heat from industrial pipes and households can also be recycled efficiently.

Though commercial TEMs have been widely operated, the bulky and rigid Peltier elements can not adapt to the human body or industrial cylindrical pipes. Therefore, flexible thermoelectric modules (FTEMs) with a deformable structure have attracted researchers' attention. Many studies have investigated the possibility of FTEMs to power wearable devices and recycle waste heat from industrial hot pipes [23][26][28][56]. The results show that FTEMs have great potential to work independently as batteries for wearable devices. But most of the research on FTEMs are concerning thermoelectric materials, substrate materials, or the design of FTEM. The mechanical strength of the joint between rigid inorganic thermoelectric legs and substrate can be easily overlooked though it is extremely important for FTEMs. Commercial Peltier elements usually consist of two rigid substrates made of ceramic, which can protect the device from external impact. However, FTEMs are designed to adapt to uneven surfaces, which means the tensile force is inevitable. Therefore, it is important to improve both the electrical property and mechanical strength of the joints simultaneously.

The commercial materials used as joints can be classified into solder paste and electrically conductive adhesive (ECA). Solders are widely used to form a permanent joint between metal workpieces. Due to the low contact resistance, solder joint possesses a favourable electrical performance. But the solder is rather costly. Pure lead solder used to be quite cheap. With the need for lead-free solder, tin becomes the main metal in solder now and it is far more expensive than lead. An economical alternative is ECA. ECAs offer the advantages of affordable substrates, low-temperature processes, excellent mechanical strength and the possibility for microdevices. But its electrical

performance is not adequate. High contact resistance hinders ECAs from large-scale use. Therefore, we decided to introduce a new ECA as binding material into FTEMs. It aims at modifying both the mechanical and electrical properties of conventional binding materials. It is named RISE (Research Institutes of Sweden) 2D-ECA, a two-dimensional anisotropic conductive adhesive.

In this work, we will compare the performance of 2D-ECA with two types of solders and ECAs. Firstly, we will study the mechanical and electrical properties of the joints between the substrate and rigid inorganic thermoelectric legs. To investigate the thermoelectric property, the materials are also used in FTEMs. We have also compared the output power of our devices with commercial Peltier elements. As a cheap substrate, polyethylene terephthalate (PET) coated with aluminum (Al) is rarely used in FTEMs. We have studied the possibility to fabricate FTEM on this cheap substrate. In the end, we propose a possible way for industrial FTEM manufacture.

2 Background

2.1 Theoretical part

2.1.1 Seebeck effect

The phenomenon of the Seebeck effect was first discovered by Estonian-German scientist Thomas Johann Seebeck in 1821 [54] when he was trying to figure out a relationship between heat and electricity in his experiment. Seebeck used two wires made of two dissimilar materials to form a circuit, as shown in fig.1, one side of the circuit was kept at a higher temperature while the other was kept at a lower temperature creating a temperature gradient. Under this condition, an electric current was formed in the circuit. The generated voltage was proportional to the temperature difference applied on the circuit and the coefficient is named as Seebeck coefficient. It is denoted as

$$\alpha_{ab} = \alpha_a - \alpha_b = \frac{\Delta V}{\Delta T} \tag{1}$$

Herein α and S are two manifestations of the Seebeck coefficient. Obviously, we can
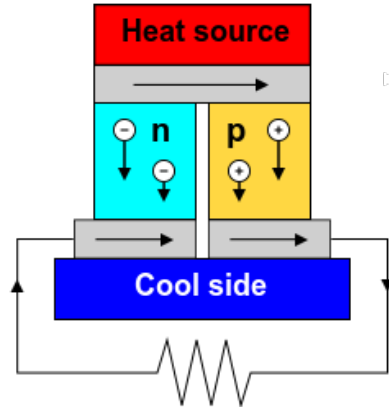

Figure 1: Seebeck effect schematic [2]

not get an absolute Seebeck coefficient of a homogeneous material as there will not be voltage generated. To obtain a Seebeck coefficient of the material, a combination of two materials is used for measurement. If the Seebeck coefficient of one of the materials is already known or it is negligibly small compared to the other material, then we can calculate the Seebeck coefficient of the latter one [37]. Another way is to exploit superconductors whose Seebeck coefficient is zero as one of the materials to form a thermocouple. However, it can only be done at extremely low temperatures. Thus, it is not a feasible method as TE modules usually work at a higher temperature.

The materials can be two dissimilar metals or two dissimilar semiconductors, but voltage generation principles are different. For semiconductors, the carrier

concentration can be represented as [7]

$$n_0 = 2(\frac{m^* k_B T}{2\pi \hbar^2})^{3/2} e^{-\frac{E_C - E_f}{k_B T}} \tag{2}$$

where m^* is the effective mass, k_B is Boltzmann constant, T is temperature, $\hbar$ is reduced Planck's constant, E_C is conduction band level and E_f is Fermi level. As we can see clearly from Eq.2, the carrier concentration increases when temperature increases. Thus, carriers on the hotter side show the trend to diffuse to the cooler side, that is how voltage is generated in the circuit formed by semiconductors. For p-type semiconductors, as the carriers are positively charged (electron holes), the Seebeck coefficient is positive. For n-type semiconductors, the Seebeck coefficient is negative as the electromotive force direction is in contradiction with the carrier diffusion direction.

The carrier concentration in metals is represented as [8]

$$n = \frac{N_A Z \rho_m}{m_a} \tag{3}$$

where N_a is the Avogadro constant, Z is the number of valence electrons, ρ_m is materials density and m_a is the mass of atom. It's clearly seen from Eq.3 that the carrier concentration in metals is not related to the temperature. Thus, the electromotive force does not come from carrier concentration difference. It is because the free electrons on the hot side have higher energy, possessing a trend to transport to the cold side.

As the carrier concentration of metals and Fermi level do not change along with temperature, hence, the Seebeck coefficient of metal is relatively small and varies from $-72 \mu V/K$ to $47 \mu V/K$ at room temperature [33]. For semiconductors, the values are much larger. For example, the Seebeck coefficient of $Pb_{15}Ge_{37}Se_{58}$ is $-1990 \mu V/K$ at room temperature. Since the performance of TE modules is proportional to the Seebeck coefficient, metals can not be used for power generation or cooling, they are mainly used for temperature sensing in thermocouples.

2.1.2 Peltier effect

Peltier effect is a reverse effect of the Seebeck effect. It was first found by French physicist Jean Charles Athanase Peltier in 1834 [36]. In his experiment, he used the same setup as Seebeck used. But temperature gradient was not applied on the circuit. Instead, the current flowed through the loop consisting of two materials and cooling as well as a heating phenomenon at the junctions, as shown in fig.2 [11].

However, Peltier couldn't completely explain this phenomenon. It was Lenz that related the rate of heat absorption or rejection to the current, which in detail is [41]

$$Q = \Pi_{AB} I = (\Pi_A - \Pi_B) I \tag{4}$$

where Π_{AB} is the Peltier coefficient and I is the electrical current. Similar to the Seebeck coefficient, the Peltier coefficient can also be positive or negative, depending

on the type of materials: n-type material has a negative Peltier coefficient while p-type material shows a positive coefficient. In n-type materials, electrons tend to leave the negative side and carry heat to the positive side, opposite to the electrical current direction. On the contrary, electron holes would carry heat to the negative side. Thus, the energy would gather at one side and emit at the other side. Due to this special property, Peltier modules can be used as both cooler and heater.
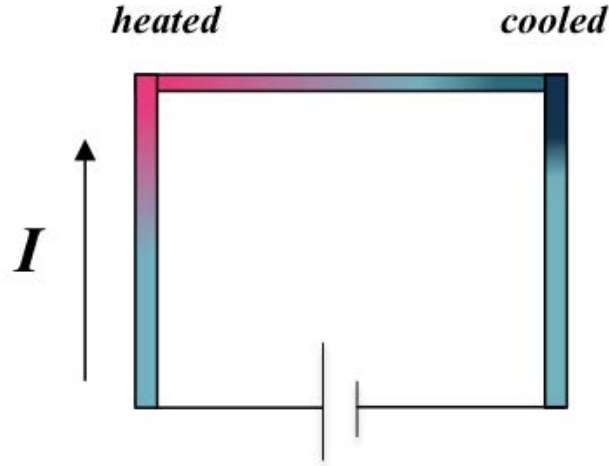

Figure 2: Peltier effect schematic

However, from Eq.4 we can see that it is hard to calculate the Peltier coefficient as the amount of heat can hardly be measured. There is a relation between the Seebeck coefficient and the Peltier coefficient, from which we can derive the Peltier coefficient:

$$\Pi = ST \tag{5}$$

This relation is known as Onsager reciprocal relation [35]. As the Seebeck coefficient of materials is easy to measure, thanks to Eq.5, we can obtain the Peltier coefficient.

2.1.3 Thomson effect

Thomson effect is the last thermoelectric effect. It was proposed and confirmed by English physicist William Thomson [47]. He predicted that when the current passed through a uniform conductor with a temperature gradient, besides joule heating caused by the conductor's resistance, there would also be heat emission or absorption phenomena at different parts of the conductor. Due to the Seebeck coefficient varying at different temperatures (we will talk about it later in detail), the phenomena can be seen as a continuous Peltier effect.

Thomson effect includes two parts: positive and negative Thomson effects. As is shown in fig.3, the current flows from A to B and there is a heat source in the middle of the bar. In case (a), when the current flows through the copper bar, heat is absorbed on the A side and evolved at the B side. This is called the positive Thomson effect. It can also be seen in other materials such as Antimony, Silver, Zinc
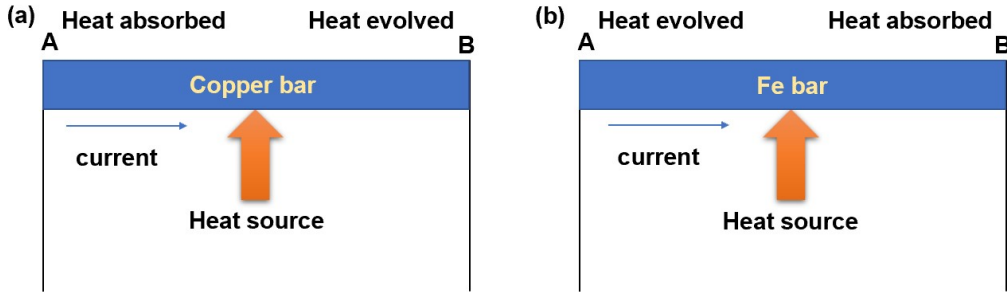
Figure 3: (a) Positive and (b) negative Thomson effect schematic

and Cadmium. Conversely, in case (b) a Fe bar, heat is evolved at the A side and absorbed at the B side. The negative Thomson effect can be observed in the case of Platinum, Bismuth, Cobalt, Nickel and Mercury [18].

Similar to Seebeck and Peltier Effect, the Thomson effect coefficient κ can also be derived. It is defined as the amount of heat absorbed or released when one ampere of current flows through the conductor at 1°C temperature difference between two nodes by one second. There is also a relationship between the Thomson effect coefficient and the Seebeck coefficient, which is

$$\kappa = T\frac{dS}{dT} \tag{6}$$

2.1.4 Thermal conduction and Joule heating

Thermal conduction and Joule heating are two irreversible processes along with the above-mentioned effects, which will affect the performance of TE modules [41]. That is to say, energy loss will be induced in TE modules and lead to the total efficiency being lower than Carnot's efficiency. Carnot efficiency is the theoretical maximum efficiency of a heat engine. It's expressed as:

$$\eta'(\%) = \frac{1 - T_{Cold}}{1 - T_{Hot}} \times 100\% \tag{7}$$

where T_{Cold} is cold side temperature and T_{Hot} is hot side temperature. Carnot efficiency only depends on the temperature difference on the two sides of a heat engine. In the presence of heat loss, Carnot efficiency can never be reached in a heat engine.

Thermal conduction is one of the heat transfer modes, the others are convection and radiation. It is a process in which heat tends to transfer from the hot side to the cold side continuously. Thermal conduction comes from the collisions of molecules' thermal motion, which promotes the heat's transfer from the hot side to the cold side. In solid, the vibration kinetic energy of particles in the crystal at the hot side is higher than on the cold side. Because of the vibrational interaction of particles, the heat inside the crystal tends to transfer from the side with larger kinetic energy to the other side with lower kinetic energy. The formula of heat loss along with the

temperature decreasing direction in one dimension is expressed as:

$$Q = -Ak\frac{dT}{dx} \tag{8}$$

where A is the cross-section area, and k is the thermal conductivity of the material. This formula is known as Fourier's law. It was proposed by French physicist Fourier in 1822. The heat loss caused by thermal conduction is proportional to the material's thermal conductivity. Thus, the material with lower thermal conductivity is required to reduce heat loss caused by thermal conduction. What's more, the performance of the TE module is highly dependent on the temperature difference between the hot and cold sides. Material with higher conductivity will also decrease the temperature, leading to poorer performance of TE modules. It is corresponding well to the former statement that low thermal conductivity material is needed.

Joule heating comes from the internal resistance of an electrical circuit. When the current flows through a conductor, heat is generated. It is known as Joule's first law:

$$P = I^2 R \tag{9}$$

It is clear that heat-generated power by the electrical conductor is positively correlated to internal resistance. Joule heating converts useful electrical energy into waste heat in TE modules. Thus, low-resistivity material is required to reduce energy loss to increase total efficiency in TE modules.

2.1.5   Thermoelectric figure of merit (ZT)

To evaluate the thermoelectrical properties of TE modules, especially efficiency, a dimensionless figure-of-merit is proposed [48]

$$ZT = \frac{S^2\sigma T}{\kappa} = \frac{S^2\sigma T}{\kappa_e + \kappa_l} \tag{10}$$

where S is the Seebeck coefficient that we have talked about before, T is the absolute temperature, σ is electrical conductivity and κ is thermal conductivity, which consists of two parts κ_e and κ_l. κ_e is the charge carrier thermal conductivity and κ_l comes from lattice (phonons and magnons). $S^2\sigma$ in the denominator part and it is described as power factor (PF). To get a high ZT value, the thermal conductivity should be low and the Seebeck coefficient as well as the electrical conductivity should be high. However, it is hard to balance the three parameters as they are interdependent, mainly determined by the scattering of charge carriers and electronic structure [12]. According to the Drude model, the electrical conductivity can be defined as

$$\sigma = ne\mu_H \tag{11}$$

where μ_H is the carrier mobility and e is the charge . And we already know that

$$\kappa = \kappa_e + \kappa_l \tag{12}$$

Here we can see that along with the increase of the carrier concentration, the electric conductivity will increase. Thermal conductivity from κ_e part, at the same time, will also increase because of the electrons' higher forward transport of energy. Usually, the electrons contribute around 1/3 to the total thermal conductivity [40].

2.1.6 Maximum efficiency and output power

A general formula to describe the energy conversion efficiency of a TEM is

$$\eta = \frac{P}{\dot{Q}_H} \tag{13}$$

where P is the generation power and $\dot{Q}_H$ is the heat flow on the hot side, it is expressed as [39]

$$\dot{Q}_H = K\Delta T + ST_h I - \frac{1}{2}I^2 R \tag{14}$$

where K is the thermal conductance, ΔT is the temperature gradient between the hot and cold side, T_h is the hot side temperature, and R is the internal resistance of the device. According to the function of Carnot efficiency, the maximum energy conversion efficiency of the TEM described by ZT is

$$\eta_{max} = \frac{T_h - T_c}{T_h} \frac{\sqrt{1 + ZT_{AB}} - 1}{\sqrt{1 + ZT_{AB}} + \frac{T_c}{T_h}} \tag{15}$$

Here we can see that a high ZT value is the key to increase the maximum efficiency.

The open-circuit voltage V_{OC} of a thermoelectric generator is expressed as

$$V_{OC} = N(S_p - S_n)\Delta T \tag{16}$$

where N is the number of legs in TEG as shown in fig.1, S_p and S_n are the Seebeck coefficient of p-type and n-type materials.

When a TEM is used as an electricity generator, external equipment will be connected to it, which will add an external resistance R_{load} inevitably to the circuit. Then the current flowing in the closed circuit will be

$$I = \frac{V_{OC}}{R_{internal} + R_{load}} \tag{17}$$

The voltage of the load will be equal to

$$V = V_{OC}\frac{R_{load}}{R_{internal} + R_{load}} \tag{18}$$

and the power of the load is equivalent to

$$P_{load} = V_{OC}^2 \frac{R_{load}}{(R_{internal} + R_{load})^2} \tag{19}$$

It follows that when the load's resistance equals the internal resistance of the module, the load's output power reaches the highest, that is

$$P_{load} = \frac{V_{OC}^2}{4R_{load}} \tag{20}$$

2.2 Thermoelectric modules basis

2.2.1 Thermoelectric materials

Though it is hard to evaluate the ZT value from a theoretical view, there are experimental values as functions of carrier concentration. As is shown in fig.4, the electrical conductivity increases with the increase of free carrier concentration, while the Seebeck coefficient shows the reverse trend. It is simple to understand that the free carriers can assist to the electrical conductivity. For the Seebeck coefficient, it can be expressed by the formula [43]

$$S = \frac{8\pi^2 k_B{}^2}{3eh^2} m^* T (\frac{\pi}{3n})^{2/3} \tag{21}$$

where h is the Plank constant. It is clear that the Seebeck coefficient will decrease with the increase of free carrier concentration.
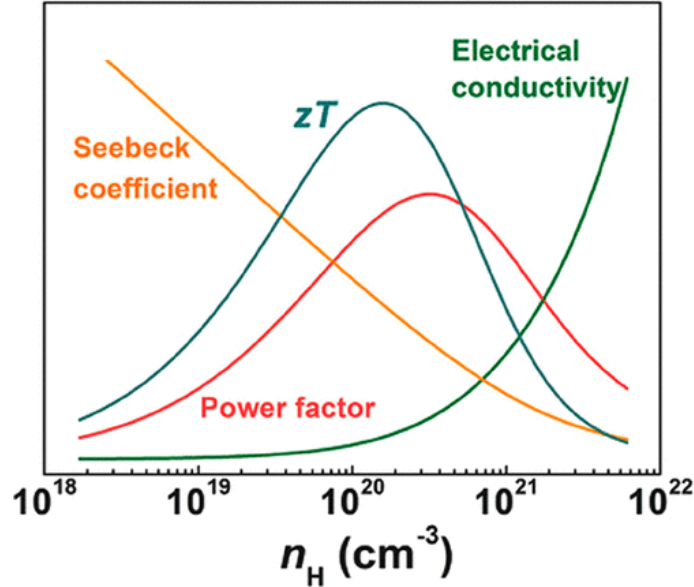

Figure 4: Schematic dependence of electrical conductivity, Seebeck coefficient, power factor, and thermal conductivity as functions of free carrier concentration [17]

ZT reaches the highest value when the free carrier is between 10^{20} cm^{-3} and 10^{21} cm^{-3}, which corresponds to semiconductor materials. Therefore, semiconductor materials are the most common thermoelectric materials that have been used in TEMs. Metals usually have superior electrical conductivity. However, their Seebeck coefficient is extremely low. What's more, high electron concentration will also lead to high thermal conductivity. Consequently, the average ZT of metals will not exceed 10^{-3} [11]. Thus, metals are mainly used in thermocouples to test temperature. Insulates can not be used as thermoelectric materials either. Though their thermal conductivity is extremely low, the electron conduction is poor, leading to poor thermoelectric properties.

Semiconductor materials are usually highly doped to reach a high ZT. If they are adjusted properly, high electrical conductivity, favourable Seebeck coefficient and acceptable thermal conductivity may be obtained. Commercial semiconductor materials can be classified into three types on the operation temperature range. The low-temperature materials are based on bismuth, doped with antimony, tellurium, and selenium at temperature up to around 450K [40]. Bi_2Te_3 is the best for power generation among the low-temperature materials, and it is also my work's experiment material. $PbTe$ is the representative material of intermediate-temperature materials with a temperature range of up to 850K. High-temperature materials are the materials that operate up to 1300K. The most used materials are silicon-germanium alloys.

In addition to the commercial materials that we discussed above, more materials have been studied recently due to the need of efficient thermoelectric materials. The groups include organic materials [31], graphene [14], Half-Heusler (hH) [38], and oxides [42]. The organic materials consist of coordination polymers, conducting polymers, carbon-based TE materials, and small molecules. The features of organic materials are low-cost, lightweight, compact and ideal for room temperature applications typically with comparatively easy manufacturing processes. But due to their low electrical conductivity and Seebeck coefficient, there is still a long way to commercialization. Graphene is also a focused material in recent studies. A research result [38]has shown that Graphene's ZT can reach 6.1 at 300K with a twisted bi-layer graphene nanoribbon junction. It is the highest value of all the materials.

2.2.2 Substrate materials

The schematic diagram and image of commercial TEM are shown in fig.5. A TEM usually consists of two substrates and a certain amount of p-type and n-type semiconductor legs. The most common substrate material for commercial products is ceramic, which has superior thermal conductivity and air tightness. But the ceramic is rigid, and can not be used as substrate materials in FTEMs. Thus, flexible materials are investigated for substrate materials in FTEMs.

There are mainly three types of flexible substrate materials: polymer, paper, and fabric. The most commonly used polymers are polydimethylsiloxane (PDMS) and Polyimide (PI). PDMS has been widely used in wearable TE devices. For example, Kyung et al [21]. used PDMS as substrate material to study the performance of mixed CNTs and Bi/Te powder as thermoelectric legs in flexible thermoelectric generators. PI is also widely applied due to its favourable high-temperature stability and mechanical properties. Paper is used as a substitution for expensive polymer substrates. It is flexible, cheap and eco-friendly. Therefore, several studies have been carried out to study paper-based TEMs. For example, Rafiq et al. [34] applied graphite pencil traces on Paper to fabricate a thermoelectric generator. Another research work shows that paper-based devices can retain their original shape after 1000 bending cycles, indicating good mechanical flexibility [57]. Fabric materials are mainly used for wearable TE devices. Due to the fabric component being similar to clothes that we wear, it can be perfectly applied to human skin. Therefore, it is a research focus now. For example, Lu et al [28]. fabricated a silk fabric-based wearable

thermoelectric generator with 12 p-n legs made of n-type Bi_2Te_3 and p-type Sb_2Te_3 nanoplates. When the temperature gradient of a range between 5 and 35 K was applied on both sides of the device, 15 nW power was generated. The open-circuit voltage is up to 10mV. Besides silk fabric, polymer fabric and glass fabric have also been used as substrate materials. Though PDMS, PI, paper, and fabric are stated as universal ones, there must be other materials that can meet our demand for flexible substrates. We still need to pursue flexible materials with low electrical and thermal conductivity as well as lightweight.
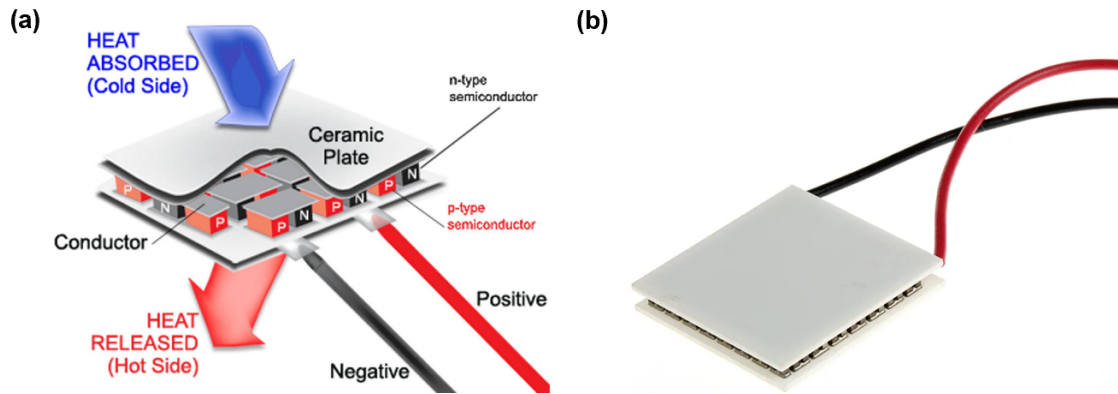

Figure 5: (a) Schematic diagram of TEM [46]. (b) Commercial Peltier element [3]

2.2.3 Binding materials

Binding materials are used to connect substrate and thermoelectric material. They can form a joint between substrate and thermocouples, acting as a medium to transport current and resisting possible tensile force. Thus, binding materials play an important role in TEMs. Commercial binding materials can be classified into solder and electrically conductive adhesive (ECA), shown in fig.6.

Solder paste usually consists of 90 % metal alloy powder and flux. Flux is used to clean the oxide of the metal during the period when the metal joint is formed. Metals are likely to oxidise when exposed to the environment and react with water, nitrogen, water, or pollutants. For example, copper may form carbonates or hydroxyl carbonates after reacting with carbon dioxide and water in the air. The chemical compound will lead to poor wettability and electrical conductivity. Therefore, the introduction of flux is important to eliminate the chemical compound. And the flux should have a proper reaction with the passivation layer. What's more, the flux should also help protect the cleaning surface from the air, promote the wetting of the surfaces, and provide adhesion between the substrate and solder.

The flux in solder paste is a mixture of flux-based material, solvent, activator and rheology aids. Rosin is commonly used as a flux base material. It is a natural organic compound extracted from pines. The main materials in rosin are terpeneoids and hydrocarbons, and abietic- and sylvic- acid play an important role in flux. Rosin is widely used in flux because of its advantages in various aspects. For example, it

destroys the passivation layer but not the copper layer. After evaporating, it will form a thin layer to protect the cleaning of the substrate surface and promote wettability. Various rosin derivatives are also used, such as dimerized resin, saponified resin or rosin-derived ester resin [9]. Among them, dymerex is a successfully modified rosin. It is a pale, acidic, thermoplastic, high-softening point resin, which means there is no colour residue after evaporation. The rosins are usually dissolved in solvents. The solvent does not only act as a carrier, but also plays an important role in the following aspects: forming a protection layer, promoting wettability, and making the application process easier. The composition of the solvent is extremely important to control the evaporation time. Because if the solvent dries too fast, the rosin may form a hard layer and could not be replaced by solder properly [25]. If the drying period is too long, it may cause sputtering when the molten solder contacts the solvent. Many factors of the solvent will influence the evaporation time, such as chemical structure, vapour pressure, the number of solvents, chemical bonds etc. Activators are also added in the flux to remove the oxide and reaction product from the metal surface. The most common activator materials are alkyl and aryl carboxylic acids. Others such as malic, adipic, and halopyridines etc. have also been investigated in a number of researches [55][44]. Rheology is used to describe the viscosity and surface tension properties of solder pastes or adhesives. It influences the printing process. Therefore, rheology aids such as castor oil derivatives, starch, and cellulose derivatives have been introduced in flux.

Metal alloys are the key part of forming a joint between metal workpieces. The melting metals under high temperature can form a joint after being cured. The most used metal alloy is tin-silver copper alloy as tin can dissolve most metals. Lead used to be an essential metal in solder paste, but it is rarely used now due to its toxicity. The most important properties of solder powder are particle shape and size. A ball-shaped particle can help decrease surface oxidation and form a good joint with the adjoining particles. While an irregular particle may block the stencil for printing. And also small-size particles can be used in printing stencils with smaller holes, improving the printability of micro components.

ECAs consist of conductive fillers and a nonconductive polymer matrix. The fillers can form a 3D structure to increase the conductivity of the nonconductive polymers. Conductive adhesives work on two conductive pathways: one is particle-particle interact and the other is electron tunnelling. For the first pathway, the conduction among the particles plays an essential role. The latter one comes from the dielectric breakdown of the matrix when the electron tunnelling between particles is close enough from electron transport. The two pathways are guarantees for low electrical resistance.

There are three types of conductive fillers: metal, ceramic, and carbon-based materials [6]. Metal fillers are composed of metal particles whose diameters are less than 20 μm. High-conductivity metals are most used in metal fillers, such as silver, copper and gold. Silver is the most used metal in commercial ECA, shown in fig.6b because of its superior high electrical conductivity, chemical stability, and lower price than gold. What's more, even silver oxide shows relatively high conductivity [27]. Copper is also an important conductive filler in electronic industries. It owns high
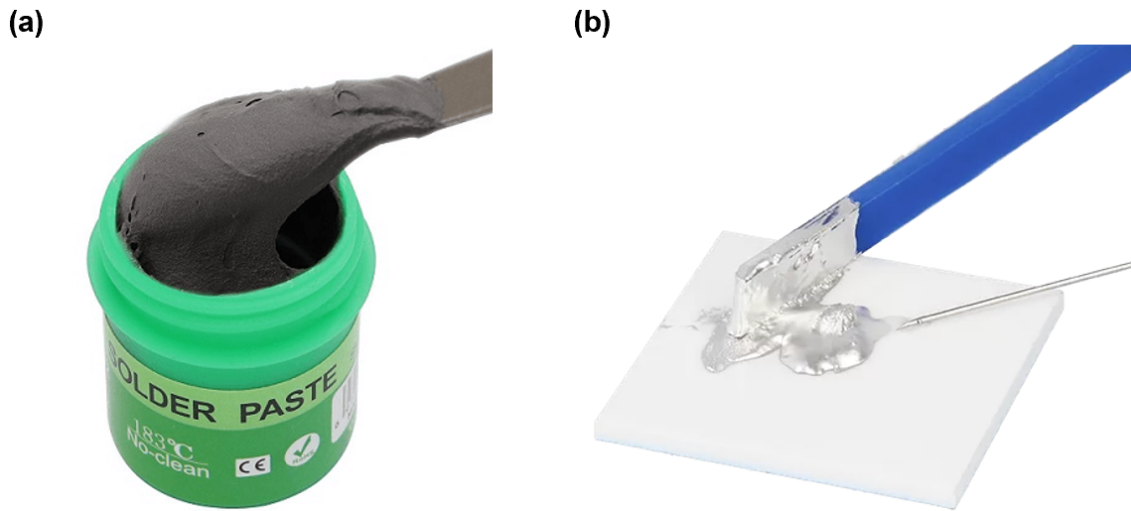
Figure 6: Commercial (a) solder and (b) electrical conductive adhesive (here is silver epoxy).

electrical and thermal conductivity, great ductility, as well as the lowest cost among metal fillers. The drawback is copper tends to oxidise when exposed to a humid environment, introducing an unfavourable increase in resistance. Gold possesses the best performance of the metal conductive fillers, but its drawback is apparent, far too expensive. Therefore, it is not quite common to use gold as a conductive filler in ECA. Nowadays metal fillers are usually fabricated in the form of nanoparticles to increase the conductivity of ECA.

Metal-coated filler is an alternative filler of the metals to lower the overall cost. The core can be either metal or nonmetal. Nonmetal cores can be polymers, carbon-based fillers, or metal-based glass. Each metal-coated filler is designed and manufactured for a unique purpose. Carbon-based fillers include graphite and carbon. When they are in the forms of nanoparticles such as carbon nanofibre (CNFs), carbon black (CB), and graphene, their electrical conductivity can be pretty high due to the high surface-to-volume ratio [19].

ECAs can be classified into isotropic conductive adhesives (ICAs) and anisotropic conductive adhesives (ACAs) according to their morphology, filler percentage, and properties. The former ECA conducts in all directions equally while the latter one only in the direction on the basis of the filler's alignment. ICAs are the most common ECAs in industries. They usually contain a high filler concentration, around 20 % to 35 % of the total volume [5]. By changing the filler concentration, the thermal and electrical conductivity of ICAs can be modified. Such a high filler concentration can help the contact between the surface and particles, leading to a higher electrical conductivity as well as electrical conduction in all directions. Epoxy is the most widely used commercial material as a non-conductive polymer. It is highly valued by its low-temperature fabrication method, superior mechanical strength, high chemical resistance, and good adhesion [32]. Though many conductive fillers have been coupled with epoxy, silver epoxy is the most common commercial product,

shown in fig.6. ICAs have been widely used in the semiconductor industry, consumer product applications, and hybrid engineering with semiconductor chips. Though the thermal and electrical conductivity of ICA can be improved by increasing the content of conductive fillers, the adhesion of the adhesive is getting poorer at the same time. To solve this problem, ACAs are invented.

The filler's concentration of conventional ACAs is lower than the ICAs, typically at around 5 % to 20 %. The electrical conduction comes from the contact between the conductive filler and the substrate as well as the bump, called single-particle bridging concept. Therefore, ACAs can only conduct in the pressurisation direction Z. For the X-Y surface, there is an electrical isolation between the particles. The particles are usually in the form of monolayer or column form with multi-layer. In the latter case, mechanical pressure should be applied to build the mechanical strength and electrical conduction between the conductive adhesive and substrate. Silicone is usually used as a polymer matrix, it possesses high thermal stability and low noncoplanarity of the layers. Epoxy is also used in ACAs because of its high mechanical strength and high reliability as well as good adhesion to other materials. Silver or silver-coated polymers are commonly used as fillers. ACAs are well suited for flexible substrates with fine-pitch bonding. However, the drawbacks of ACAs such as low thermal and electrical conductivity, degradation under highly humid environments, and unstable contact have hindered their large-scale application. Therefore, the idea of solderable anisotropic conductive adhesives (SACAs) has been proposed. SACAs have the advantages of both solder and ECA [52][53].

2.2.4 TEM designs

The structure shown in fig.5 is the most commonly used TEM design. It is a mixed structure combined with heat flowing vertically and current transmission laterally. When a temperature gradient is applied on the two substrates, current will be generated in pairs of legs and transmitted along with the direction of the circuit. However, this design can not be directly used in FTEMs when the substrate materials are not stretchable enough. In this case, when the device is bent, the joint between thermoelectric legs and substrates may not bear the tensile force and breaks. Thus, many approaches have been investigated for stretchable devices.

Fig.7a illustrates a unique design of FTEM based on rigid inorganic bulk materials [15]. Researchers used a copper wire electrode to connect two thermoelectric legs. Thanks to the flexibility of the copper wire, the two connected units can be twisted easily. They fabricated a device based on ten pairs of units by repeating the process. The theoretical result showed that the performance of FTEM was as good as the conventional modules. In addition to the design of thermoelectric legs, the substrates can also be modified to fabricate FTEM. As shown in fig.7b, Wang et al. [49] drilled a number of holes in flexible printed circuit board (FPCB) to strengthen its flexibility as well as improve heat transfer from human skin. And they also applied a thin flexible PDMS layer as the top substrate. After these methods, flexibility was enhanced greatly. The result demonstrated that the module can be used as a battery for powering electronics and/or sensors. Though PDMS is known for its

flexibility, its thermal conductivity is quite low, around $0.16 W/mK$ [16]. It can not meet our demand for fast heat dispassion to increase the temperature gradient. To solve this, Kuang et al. [24] applied heteromorphic electrodes as the top substrate. On the one hand, the flexibility was enhanced as there was no filling material, which would introduce tensile force inevitably. On the other hand, heteromorphic electrodes could act as heat sinks. It was a great way to kill two birds with one stone. As a consequence, the power of modifying devices with heteromorphic electrodes was 41 times higher than conventional devices due to the improved heat dissipation.
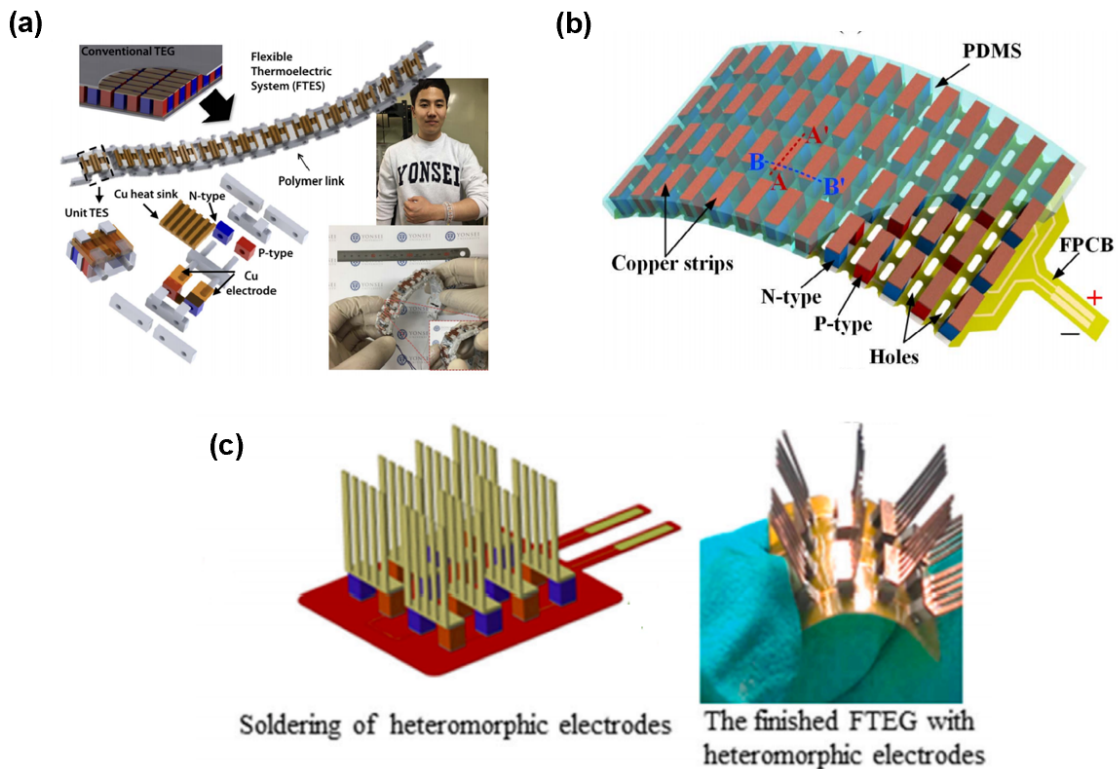
Figure 7: Three FTEM designs fabricated with (a) ten pairs of units connected by flexible copper wire electrodes [15]; (b) pore-structure FPCB and thin-layer PDMS as substrates [49]; (c) heteromorphic electrodes [24].

In addition to the structure that we disscussed above, a planar structure is also very common. Fig.8 demonstrates the schematic diagram of a planar-structure FTEM [20]. Herein, the thermoelectric materials are printed, patterned or deposited on the substrate. Therefore, the thickness and length of thermocouples can be easily manipulated. The volume of the device is much lower and more convenient to carry. But the temperature gradient comes from the length/width of the substrate, not from the ideal vertical direction. As a result, the energy conversion efficiency is lower than the mixed structure.
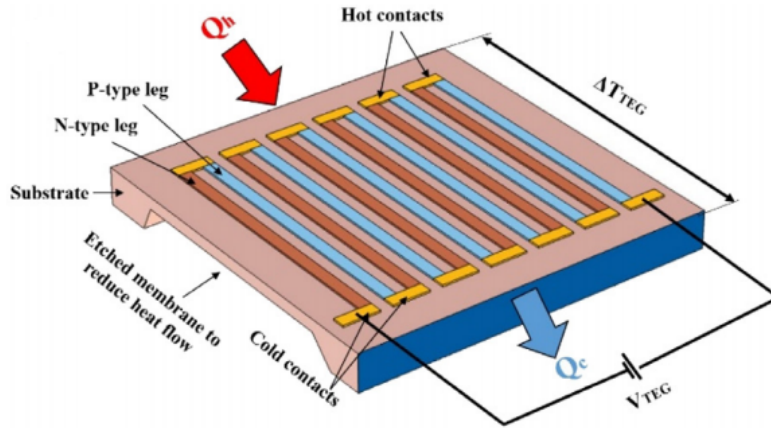
Figure 8: Schematic diagram of planar-structure FTEM [20]

2.2.5 Common applications

TEMs are mainly used for power generation, heating and cooling based on the Seebeck and Peltier effect. Commercial Peltier elements have been widely used as cooler in many scenes. For example, a TE freezer can be used for medical purposes as it is safe and does not produce harmful materials. It can produce low temperatures for the preservation and transportation of vaccination, blood serum, biological products etc. Besides this, Peltier elements can also be used to cool electronic devices. Many electronic devices work at high power including computers, sensors, charge-coupled devices (CCD) etc. and their working temperature will rise inevitably. But these devices usually require a low-temperature working environment to maintain high efficiency and sensitivity. Thus, a cooling system is needed to improve the performance and working time. However, conventional coolers are not compact and usually take up considerable room in the devices, enlarging their weight and volume unintentionally. On the contrary TE coolers are known for compactness in size, no moving parts, no noise and long working time. Therefore, they can be perfectly used in high-power devices. For example, Sun et al. [45] designed a cooling system based on TE coolers. The result demonstrated that the cooling capacity has improved by 73.54 % and the electricity consumption has been reduced by 42.2 % when producing the same amount of cooling compared to a conventional device cooling system.

In addition to cooling, TEMs are also good power generators. Due to the special Seebeck effect, TEMs can directly convert heat energy into electricity without any extra rotating part. But conventional TEMs are rigid, and can not suit the surface of uneven objects such as pipes and the human body. Therefore, FTEMs are mainly used as power generators in many scenarios. As is shown in fig.9, the applications of FTEMs can be classified into four parts: industrial waste heat harvester, clothes system, finger touch sensor and battery for medical sensors. For example, Li et al. [26] demonstrated high-power conformal half-Heusler (hH) TE modules for high-temperature applications and integrated them on fuel gas platforms to collect waste heat. The TE module consisted of 72-couple hH legs. As a result, the device showed
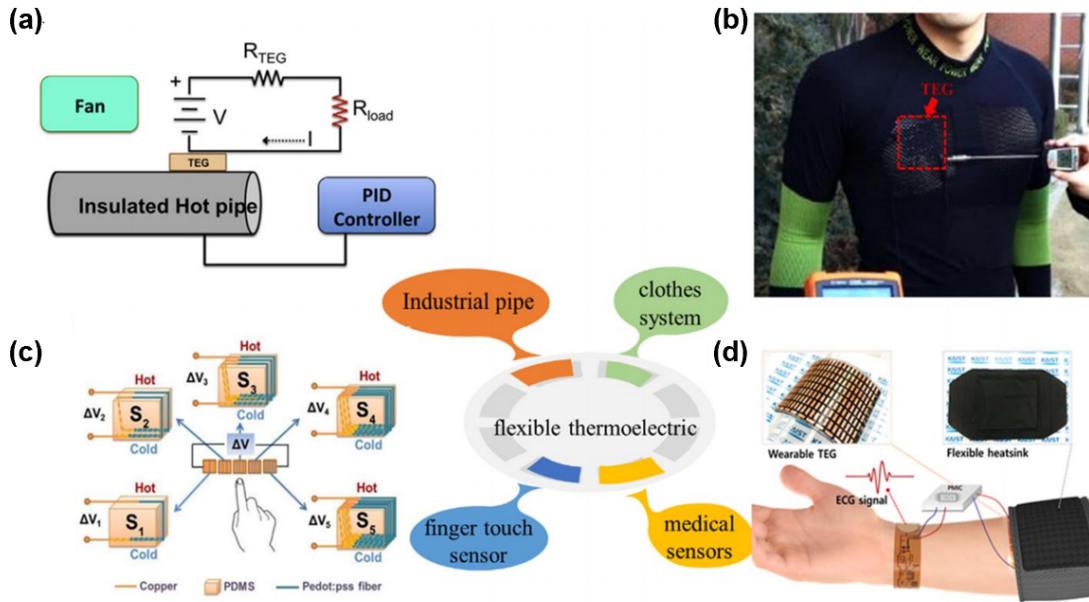
Figure 9: FTEM applications: (a) Collecting waste heat from industrial hot pipes [29]. (b) Collecting energy from the human body [23]. (c) Finger touch sensor [51]. (d) Battery to provide electricity for medical sensors [22].

favourable performance on energy harvesting with a high power density of 3.13 W/cm^{-2} and total output power of 56.6 W at the temperature gradient of 570 K. As the factories always produce a large amount of waste heat while working, FTEMs will play an important role to convert the waste heat to electricity. As we have talked about before, the fabric can be used as FTEM substrate material. Thus, researchers have also investigated fabric-based TEMs. Lu et al. [28] designed and fabricated a wearable device by depositing 12 pairs of thermocouples with nanoscale TE materials on silk fabric substrate. The maximum open-circuit voltage and output power of the device are 10 mV and 10 nW respectively at $\Delta T = 30K$. FTEMs can also be used as finger touch sensors. According to Eq.18, the temperature gradient can be calculated from the open-circuit voltage and the Seebeck coefficient. Based on this, FTEMs can be used to test human body temperature when their Seebeck coefficient is already known. Zeng et al. [56]used nylon telluride silver telluride nanowires as TE materials and fabricated a self-powered temperature sensor with a maximum high PF of 315.1 $nWm^{-1}K^{-2}$. The sensitivity is also very high, its response and rest time are around 1.05 and 2.1s, showing a promising future in the micro temperature testing field. The last application of FTEM is in the wearable device field. It is mainly used as a battery to supply power to wearable devices. For example, Kim et al. [23] designed and fabricated a flexible fibreglass-based TEM, the output power density of which is around 28 mWg^{-1}. It can be integrated with wearable devices such as medical sensors and smartwatches. What's more, Wang et al. [49] designed a novel wearable TEG with 52 pairs of cubic-shaped thermoelectric legs, shown in fig.7b. The device can generate a maximum output power of 37.2 mW at $\Delta T = 18K$, while using the

human body as the heat source. And then they found the device can provide stable electricity for a 3-axis miniaturized accelerometer. With the rapid development of IoT, we can imagine the prospective future of wearable FTEMs.

3 Research material and methods

3.1 Research methods

3.1.1 Four point probe test

The potential probe is the most common method to measure the resistivity of a sample and it can be divided into four point probe test and two point probe test. The four point probe technology is also named Wenner method as it is firstly invented by Wenner in 1916 to measure the earth's resistivity [50]. The schematic diagram of four point probe test is shown in fig.10a. The voltage drop is gauged between the two inner sensors. Current flowing across the sample is measured in the edge by two outer contacts. Hence the contact resistance of the probe and sample can be ignored. Therefore, four point probe technique is an accurate method regardless of contact resistance for resistance test. The resistance is simply calculated by

$$R = \frac{V}{I} \tag{22}$$

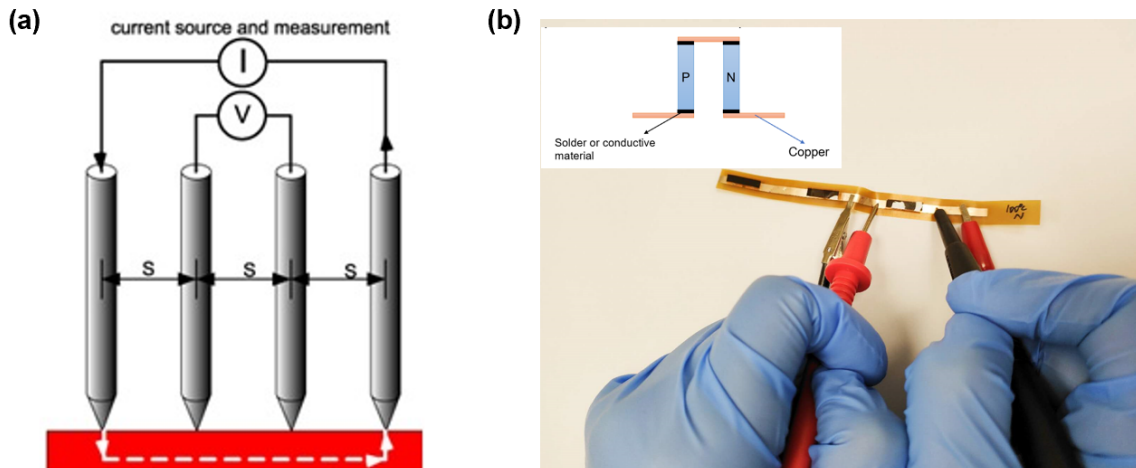Though two point probe test is also widely used for sample's resistance measurement

Figure 10: (a) Schematic diagram [4]of four point probe measurement (b) Our experimental setup

(such as multimeter), the contact and spreading resistance in two point probe test is large. Therefore, two point probe test can not provide an accurate result. In our experiment, the total resistance of the sample is extremely low. Thus, the contact and spreading resistance would affect the true value.

To obtain a precise resistance value, we decided to use four point probe test as the measurement method. As is shown in fig.10b, we chose a piece of module as research object. The sample consists of a pair of thermoelectric legs, four solder or electrical conductive adhesive joints and a certain distance of copper. Hence we can analyze the resistance of each part precisely. Similar to the schematic diagram, the inner two probes tested the voltage and the outer two probes tested the current flows through

the circuit. We have also used DC power supply (E3632A, DC Power Supply, Agilent) to provide voltage and two multimeters (34401A Multimeter, Hewlett Packard) to test the voltage and current respectively. The final resistance was obtained from Eq.22. Thus, we can compare the electrical properties of different materials.

3.1.2 Tensile test

Tensile test is a fundamental method in material science and engineering. The sample bears an increasing external force until failure. By recording the whole process, researchers can directly get the samples' ultimate tensile strength, breaking strength, maximum elongation and reduction in area [13]. In our case, the mechanical strength of the joints are crucial for FTEMs. Therefore, we want to know the largest force that samples made of different binding materials can bear.
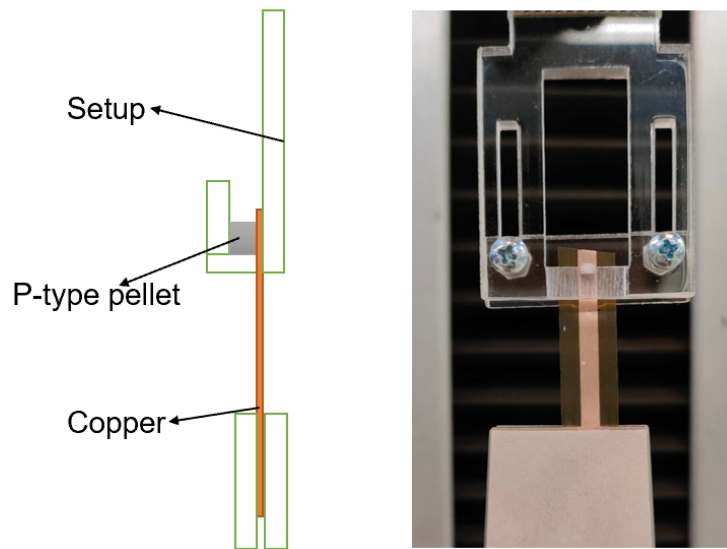

Figure 11: Schematic diagram from lateral view and real picture of the tensile test setup

The picture of the setup is shown in fig.11. The sample consists of a p-type pellet and copper substrate. Left figure is the schematic diagram from lateral view. We firstly fixed the sample in the groove (shown in right figure) of the setup. Then a tensile force is applied on the top side until the sample breaks at the joint. Since the sample's largest bearing tensile force is usually no more than 50N, we chose a 100N sensor in the setup to get a more accurate value. The setup is connected to a computer. Therefore, we can directly record the tensile force from the specific software. By comparing the maximum tensile force before breaking, we can finally compare the mechanical strength of each sample.

3.1.3 SEM and EDX

Scanning electron microscope (SEM) and energy dispersive X-Ray analysis (EDX) were used to study the information about breaking part from tensile test. The

electron gun in SEM generates an electron beam to scan the sample's surface. Then the electrons interact with the atoms in the sample and reflex different signals. For example, back-scattered electrons (BSE) can provide information about the differences in atomical number and secondary electrons (SE) help to observe the morphology of the sample's surface.

EDX is usually used for chemical characterization or elemental analysis. It is an analytical technique based on analyzing X-ray emitted from the sample. When the electron beam hits the surface of the sample, the electrons in the shell will be knocked off, leaving a positively charged electron hole. Electrons with higher energy from outer shell will fill the hole, while releasing extra energy in the form of X-ray. The detector can recognize the elements and their content. The working principle comes from Moseley's law [10]:

$$\sqrt{\nu} \propto Z \tag{23}$$

where ν is the frequency of X-ray, and Z is atomic number. It illustrates that the square root of X-ray's frequency is proportional to the atomic number. Therefore, EDX can be used for element analyzing. In our experiment, we used SEM and EDX to analyze the breaking point.

3.1.4 Output power test

The power generator performance was tested in the setup shown in fig.12. The setup is composed of several parts: a hotplate for heating the device's substrate; a heat sink to cool down the other side and thus provide a temperature gradient; a breadboard used to change the load's resistance; a temperature recorder to test both hot and cold side temperatures; a data acquisition to measure the voltage of the external load. The picture of our setup is shown in fig.12

Herein, we were not able to control the cold side temperature precisely by the heat sink. The cold side temperature was maintained at a relatively fixed value after long-time operation for each sample. But the hot side temperature is fixed. We set the hot side temperatures to be 50ºC, 60ºC, 70ºC, and 80ºC. A breadboard with several different resistors is used to adjust the load's resistance. It includes 1.7, 3.5, 4.9, 6.2, 7.8, 9.9, 19.7, 29.5, 39.4, 49.1, 54 and 56.9 ohms. The resistors are connected to the module in series. Two sensing wires from the top and bottom substrates of the module are connected to the temperature reader. Here we fixed the position of each sample and the wires to minimize the measurement error. A data acquisition is used to record the load voltage. As we can not read the current in the circuit directly, we calculated the current from the load's voltage and resistance by Ohm's law.

3.1.5 Open-circuit voltage test

To test the V_{OC} versus temperature gradient, we selected p-n couples with two substrates as samples. Then the different temperatures were applied on the two substrates of the sample. Two wires are connected to the sample to measure the open-circuit voltage. As a result, we can obtain the voltage-temperature gradient results. The diagram of the setup is shown in fig.13.
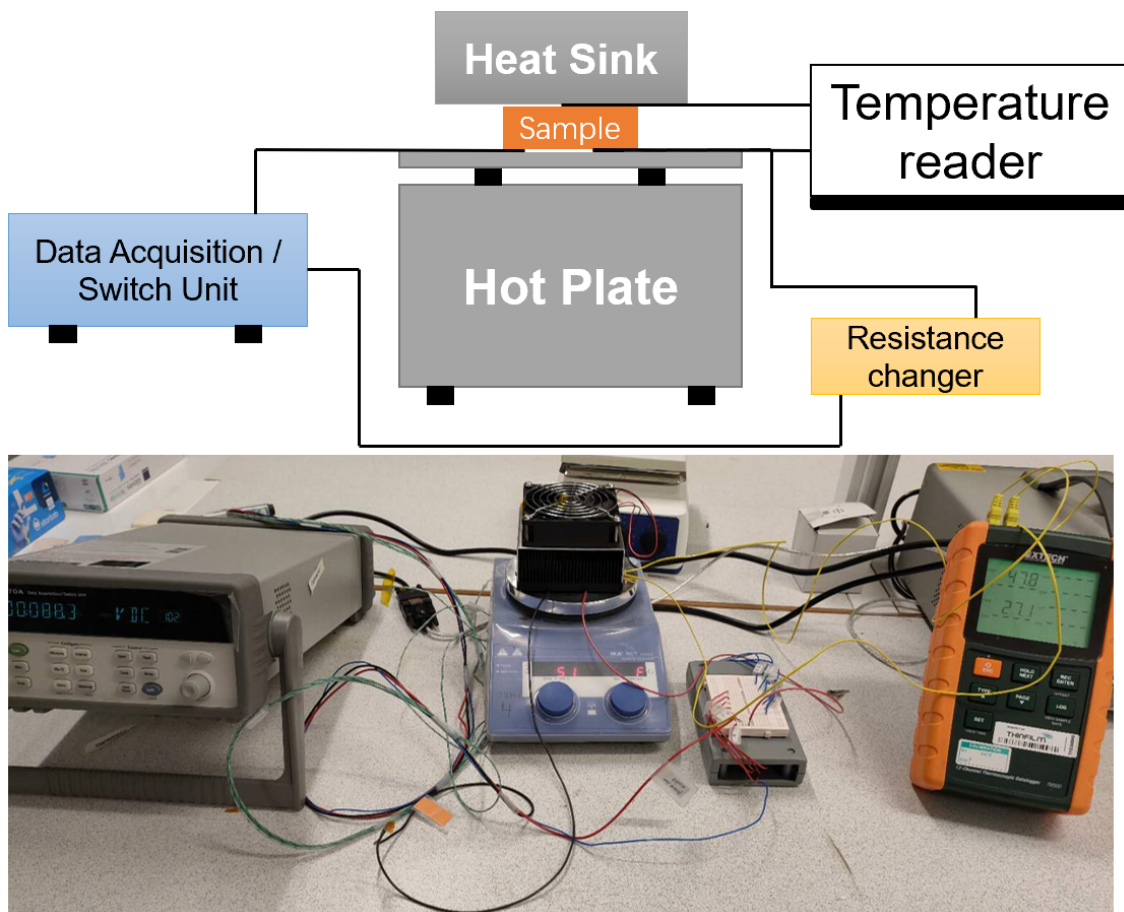
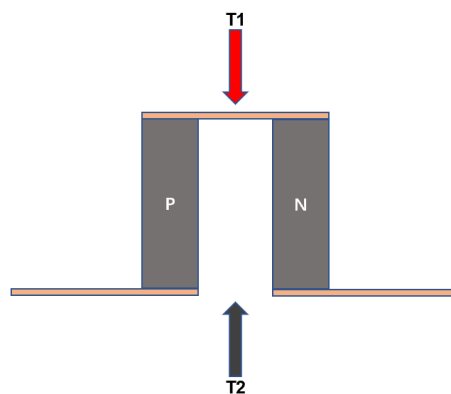Figure 12: Diagram of the output power test setup.

Figure 13: Schematic diagram of the voltage-temperature test setup

3.2 Research materials

Thermoelectric legs were purchased from a Russian company. The size of the bottom area is 1.5±0.02 mm, while the height is 2.0±0.02 mm. Its electrical conductivity at 300K is $1 \times 10^5 (\Omega m)^{-1}$. The substrates are Polyimide (PI) coated with copper. Solder pastes (OM550 and OM353) were purchased from Alpha. OM550 is a low-

temperature solder paste and OM353 is a standard-temperature solder paste. ECAs were purchased from ATOM including ATOM907 and ATOM917. The research ECA was named 2D-ECA, and synthesized by Linköping University and Research Institutes of Sweden (RISE). The commercial Peltier was purchased from Digikey, type 56460-501.

3.3 Fabrication methods

The fabrication process of FTEMs is shown in fig.14. Firstly, the solder pastes or the ECAs are deposited on the substrates by a stencil. Then the pellets are placed on the binding materials in the order of p-type and n-type. The top substrate is cut from a full-size substrate that has already been printed with binding materials. After the top substrate placed on the pellets, the prepared sample is finished. The last step is to cure the sample. Reflow soldering is used to cure the solder paste, while ECA based samples are put in the oven at 100℃. The picture of the final product is shown in fig.15
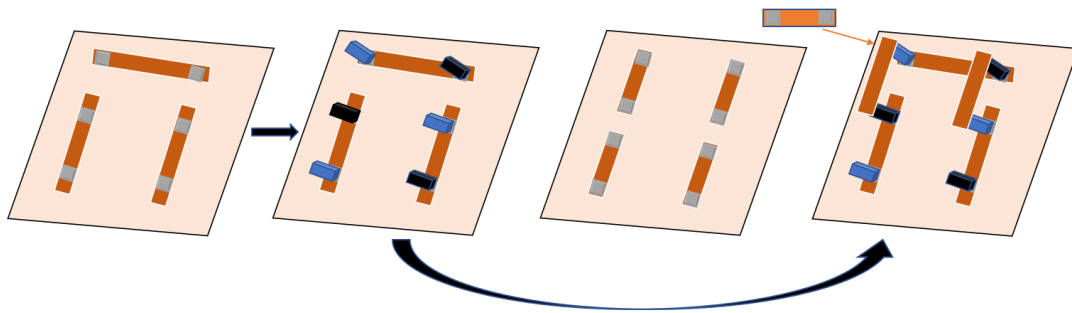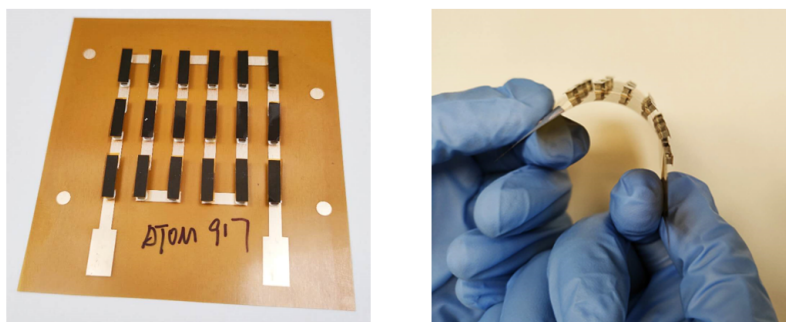

Figure 14: Fabrication process

Figure 15: Pictures of the device

4 Results

4.1 Single joints test

4.1.1 Mechanical strength and electrical resistance

We first conducted mechanical strength and electrical resistance characterization, relative results are shown in fig.16 and Table.1. X-axis represents different joint materials and the two y-axis represent the maximum tensile force divided by the contact area (1.5mm×1.5mm) before sample breaking and electrical resistance. The outside box represents where 25% to 75% results exit. The line inside the box is the mean value and the top and bottom dots represents the highest and lowest value. Herein, the mean value is extracted from the test results of ten samples.

Table 1: Mechanical strength and electrical resistance result

Material	2D-ECA	ATOM907	ATOM917	OM550	OM353
Strength (N/mm^2)	10.26	10.72	4.65	9.50	5.11
Resistance (ohms)	1.071	0.442	3.681	0.026	0.028

As shown in Table.1, 2D-ECA shows an excellent mechanical strength. The mean mechanical strength value of 2D-ECA is around 10.26 N/mm^2, similar to the results of ATOM907 and OM550. Moreover, the mechanical strength of ATOM917 and OM353 is relatively lower, around 5 N/mm^2. Thus, the mechanical strength of 2D-ECA is far better than the ordinary commercial solder paste and ECA, almost double of them. Since mechanical strength is an important factor for FTEMs, 2D-ECA showed great potential in working as a joint material to provide protection for the connection between the pellet and substrate. In conclusion, the performance of 2D-ECA is as good as exceptional commercial solder pastes and ECAs and even better than ordinary commercial products.

In addition, we found that the breaking position of the solder paste joint and 2D-ECA joint was not the same. As is shown in fig.A1, the pellet coated with 2D-ECA breaks at the interface between 2D-ECA and copper sheet, which means the adhesive force between 2D-ECA and copper sheet is lower than 2D-ECA and pellet. However, the pellet coated with solder pastes (including OM550 and OM353) seems to break in the pellet part visually, since there is pellet structure remaining on the substrate. A sketch shown in fig.17 explains the phenomenon. As we discussed in the theoretical part, the working principle of ECA and solder paste is not the same. Solder pastes form a joint by melting metals while ECAs stick the targets, providing an adhesive force. Thus, it is possible that the interaction between solder paste and BiTe weakens the mechanical strength of the pellet. To obtain a more precise result, we conducted a further study to investigate the position of the breaking point. Herein, we used SEM and EDX to conduct our research.

To investigate where the pellet breaks, we first conducted SEM to observe the images of the breaking layer. Since it is clearly seen that 2D-ECA based samples broke at the interface between 2D-ECA and the substrate, we only researched solder
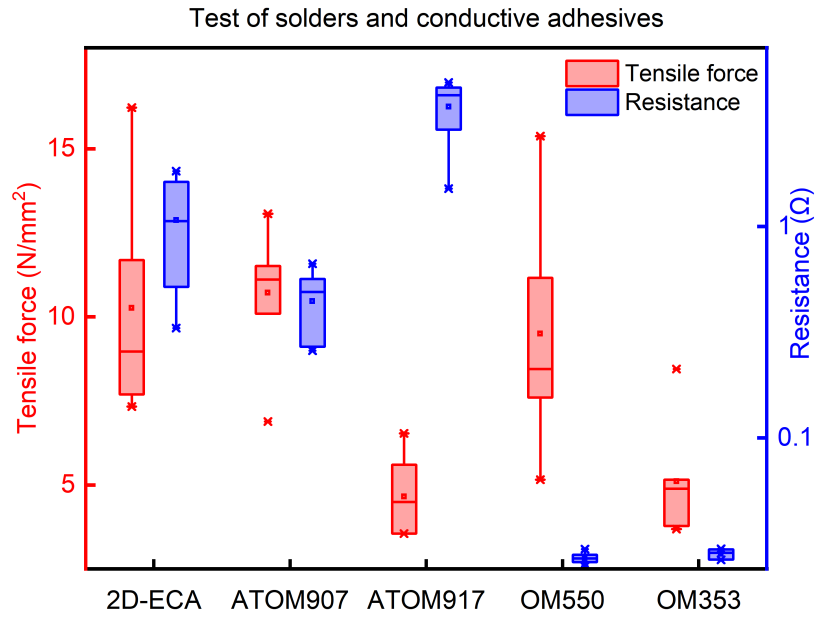
Figure 16: Mechanical strength and electrical resistance test results of different joint material-based samples.
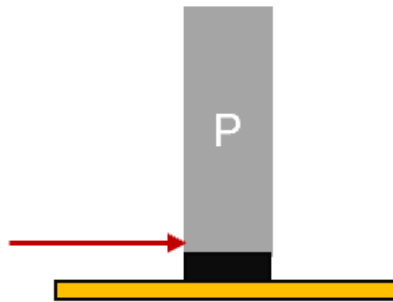

Figure 17: A sketch explaining where the fracture point might be. The black part is the binding material.

paste based samples. We collected both the substrate and pellet for SEM tests as a control group. SEM results are shown in fig.18. Herein. in order to get a more general result, we chose several positions at the substrate and pellet under-surface for SEM tests. As is seen in fig.18, there are clear crystal layers at the pellet under-surfaces. Since the main component of the pellet is BiTe, thus the layers are mostly likely to be BiTe crystals. Moreover, the SEM figures of BiTe in [30] further confirmed that the crystal layer is BiTe. As a result, the existence of BiTe shows that the breaking position is not in the solder paste section. Moreover, similar crystal layers were also observed on the substrate. As shown in fig.18, BiTe layers were seen at all the positions. If the pellet breaks in the solder part or the intermediate layer between the substrate and solder, there will be no BiTe crystal layer on SEM images.
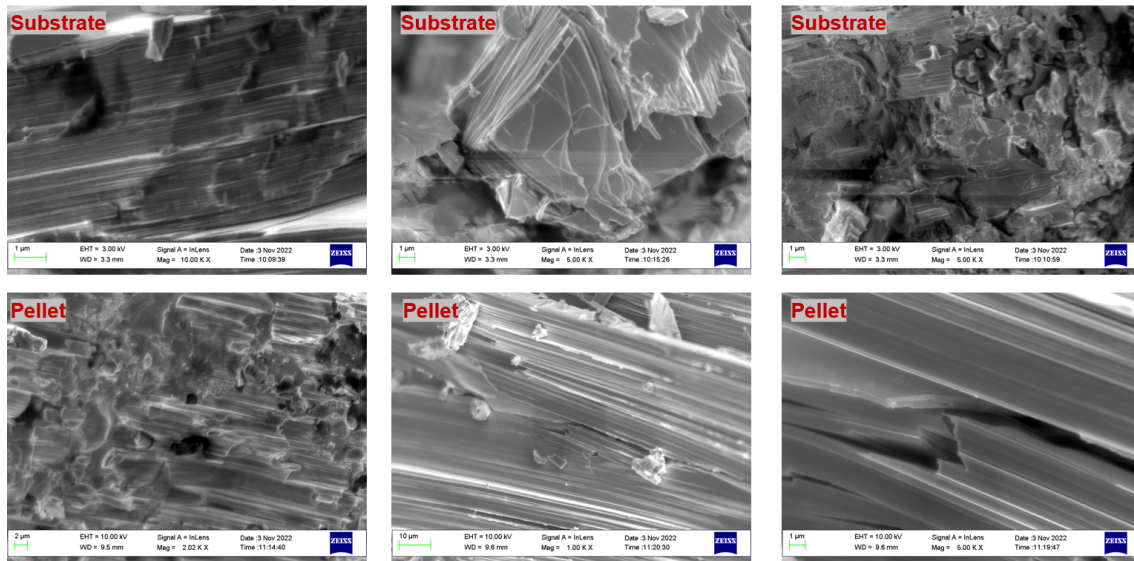
Figure 18: SEM images of the breaking layer

Hence, combining SEM results from both the substrate and pellet, it is clear that the breaking position is in the pellet section.
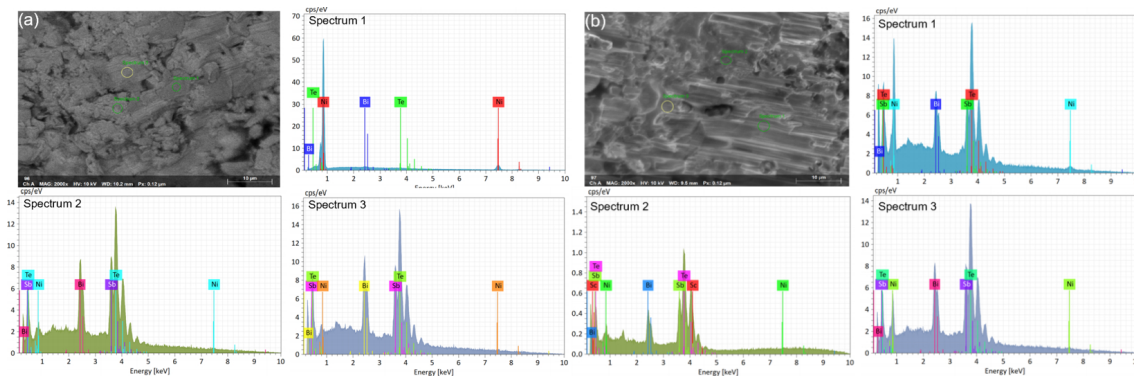

Figure 19: EDX analysis of (a) substrate surface and (b) pellet under-surface

We also exploited the EDX method to identify the elemental composition of both the substrate surface and pellet from the breaking samples. We chose three different positions of the samples for elemental analysis, relative results are shown in fig.19. For the substrate surface, detected elements are pellet constituent elements, such as Bi, Te, Ni, and Sb. However, the main component of the solder paste we used is Sn, which was not found in the EDX result. Moreover, EDX analysis of the pellet under-surface showed that there were also no significant solder elements in the pellet part. Combining the EDX results from the substrate and pellet, it is clear that the pellet broke at its main body, rather than the solder layer or intermediate layer between the copper sheet and solder layer. Thus, the solder paste has weakened the mechanical strength of the pellet itself, leading to a break at its main body. At the same time, 2D-ECA has no negative impact on the mechanical strength of the

pellet itself. Hence, 2D-ECA has a greater potential to form a more stable joint if its adhesion on the copper substrate could be promoted in further research.

The electrical resistance of 2D-ECA is shown in Table.1. For a 2D-ECA based junction composed of both p-type and n-type thermoelectric legs, its mean resistance is around 1.071 ohms, while the value is only around 0.028 ohms for the solder based junction. The majority of resistance comes from the contact resistance between 2D-ECA and thermoelectric legs or the copper substrate. Since the solder paste forms a joint by melting the target metals, its contact resistance is rather low, leading to low electrical resistance. The poorer performance of 2D-ECA comes from its working mechanism, which is unavoidable. However, 2D-ECA doesn't show a greater performance compared to other commercial ECAs. The mean resistance of the sample @ ATOM907 is 0.442 ohms, lower than 2D-ECA, while the result of the sample @ ATOM917 is 3.681 ohms. Therefore, 2D-ECA possesses a better performance on electrical conductivity than ATOM917 but a poorer one compared with the excellent commercial ATOM907 ECA. Thus, 2D-ECA still needs improvement in its electrical conductivity performance.

4.1.2 Voltage-Temperature test

Open-circuit voltage versus temperature gradient test was further conducted by the setup shown in fig.13. We applied different temperatures on the two substrates of the sample to create the temperature gradient. As a result, different temperature gradients were achieved in our experiment. The result is shown in fig.20. According to the formula $V_{OC} = N(S_p - S_n)\Delta T$, it is clear that the open circuit voltage is proportional to the temperature gradient. After linear fitting, the slope was obtained to study how V_{OC} changes with per temperature gradient. The slope is 0.139 mV/K, which means per temperature gradient will create 0.139 mV in a p-n couple. The device we fabricated contains 18 couples. Therefore, the theoretical open-circuit of the device will be 2.502 mV.

4.2 Output power

To investigate the thermoelectric properties of 2D-ECA, we further performed output power test on 2D-ECA based devices, results are shown in Table.2 and fig.21. Fig.21a shows the voltage-current curves under different temperatures, fig.21b shows the output power versus load resistance, and Table.2 shows the maximum output power under different temperatures.

Table 2: Maximum output power

Heat source temperature (℃)	50	60	70	80
Temperature gradient (℃)	11.6	19.1	25.3	28.6
Maximum power (mW)	0.20	0.45	0.83	1.04

It can be seen here the maximum output power is under 1 mW when the heat source temperature is under 80 ℃, which is not enough for a wearable device, while
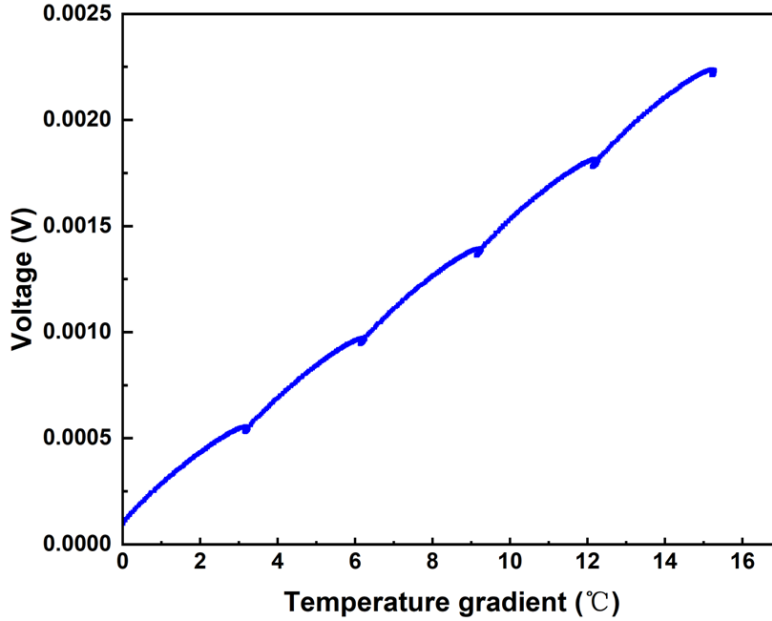
Figure 20: Voltage versus temperature gradient curves.

the voltage is also too low. Therefore, a voltage step-up is needed to upgrade the voltage to a required voltage of a device. Moreover, a dense pellet arrangement on the substrate can also be used to improve the total output power. In fact, commercial Peltier elements usually contain exceedingly dense thermoelectric legs to achieve the highest output power in a limited area.

It is worth noticing that the internal resistance of 2D-ECA based device is around 4.5 ohms under 50 ℃. However, the previous resistance test shows that the resistance of a p-n couple is around 1 ohms. The device consists of 18 p-n couples, which means the theoretical internal resistance will be around 18 ohms. Therefore, the resistance of the device reduces while working under high temperature. We further calculated the contact resistance between 2D-ECA and substrate or TE leg. The total internal resistance consists of resistance from copper sheets, 18 p-n legs, and 72 contact layers. After subtracting the resistance of copper sheets and TE legs, we obtained the contact resistance, which is around 0.052 ohms.

In addition, we also compared the output power of 2D-ECA based devices with other materials based devices, commercial Peltier element and non-flexible TEMs. The commercial Peltier element contains 144 thermoelectric legs. However, the devices we fabricated only contain 36 thermoelectric legs. To standardize the results, we recalculated the output power of the commercial device. The I-V curves and power-resistance curves are shown in fig.A2 and fig.A3, and the output power comparison is shown in fig.22 and Table.3. Herein, the standard device refers to the non-flexible TEM fabricated with OM550.

As we can see from fig.22, the output power of 2D-ECA based device shows a better performance than the commercial ECA ATOM 907 but a poorer performance than the solder. It is worth noticing that though ATOM907 shows a relatively
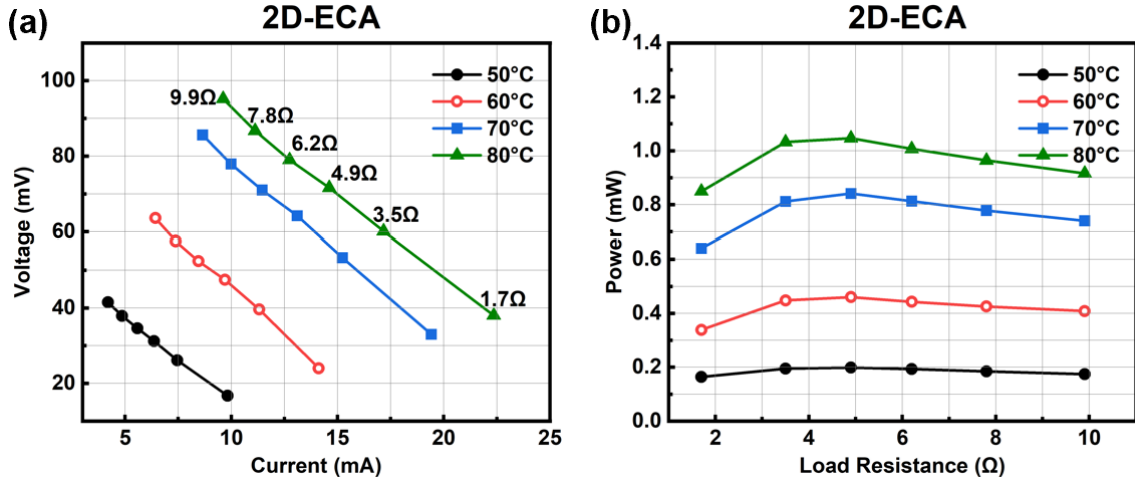
Figure 21: (a) I-V curve and (b) output power versus different load resistance

Table 3: Maximum output power values comparison (unit: mW)

Device\Temperature (℃)	50	60	70	80
2D-ECA	0.20	0.45	0.83	1.04
Commercial	0.45	0.90	1.68	3.19
Standard	1.11	2.55	4.20	6.02
OM550	1.25	2.77	4.76	7.21
ATOM907	0.03	0.04	0.07	0.11

lower resistance in previous research, its resistance rises much after heating to 50 ℃, showing a poor unstable electrical contact resistance. The result shows that its internal resistance is extremely high, around 60 ohms. Therefore, internal resistance is a key factor that hinders the thermoelectric properties of ECA based devices. Nevertheless, 2D-ECA still shows a lower electrical resistance than commercial ECAs, leading to higher output power. It is also worth noticing that OM550 based device shows the highest output power, superior to the commercial Peltier element and standard one. It indicates our design of the FTEM is a success. The improved performance comes from better heat dissipation than the conventional TEM.

4.3   Aluminium substrate

The devices that we talked about before were all fabricated on Copper-Polyimide (PI) substrates. However, both copper and PI are expensive materials, leading to high costs. Therefore, cheaper substrates are desired to lower the total cost. One alternative is aluminium (Al) - polyethene terephthalate (PET) substrate as both Al and PET are inexpensive materials. Though it is an economical alternative for FTEMs, normal solders paste can not be soldered on Al substrate, hindering it from large-scale use. To solder on Al substrates, Zinc Chloride is especially needed as a compound for the flux to effectively form a joint. We have also exploited our solder pastes to solder on the Al substrates and it failed to form a joint. In contrast to
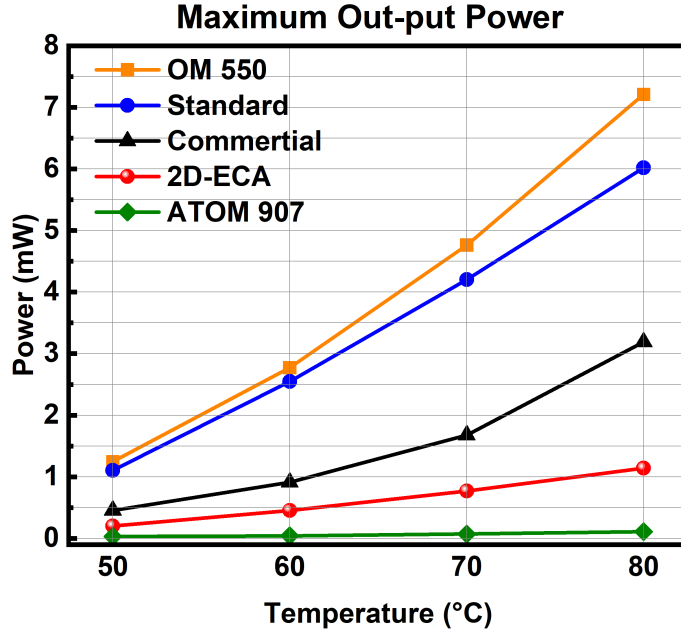
Figure 22: Maximum output power comparison

solder paste, ECAs can directly work on Al substrates. Hence, we have also tried to fabricate thermoelectric legs on Al-PET substrates. Herein, we mainly compare the output power of copper and aluminium substrate devices. The results are shown in Table.4 and fig.23. The figure of an Al substrate sample and its Current-voltage is shown in fig.23a, and the comparison of maximum output power in different devices is shown in fig.23b.

Table 4: Maximum output power of Al substrate devices

Temperature (℃)	50	60	70	80
Internal resistance (ohms)	79.912	86.071	100.172	126.149
Maximum output power (mW)	0.014	0.028	0.041	0.043

As we can see from Table.4, the maximum output power of the Al substrate device is rather low, around 0.014 mW at 50 ℃, while the copper substrate device shows 0.2 mW. It indicates the maximum output power of the Al substrate device is around 14 times lower than normal copper substrate device. The enormous difference comes from the high internal resistance of Al substrate device. It is known that aluminium is easy to react with oxygen in the air and forms a thin aluminium oxide layer on the surface of pure aluminium. However, aluminium oxide possesses a high electrical resistivity. As a result, the aluminium oxide layer between 2D-ECA and the Al substrate caused a prodigious contact resistance. That is why the Al substrate device shows high internal resistance, thus leading to poor performance. To overcome this drawback, special materials may be needed in 2D-ECA to remove the aluminium oxide on the surface. Other effective methods can also be applied to remove the
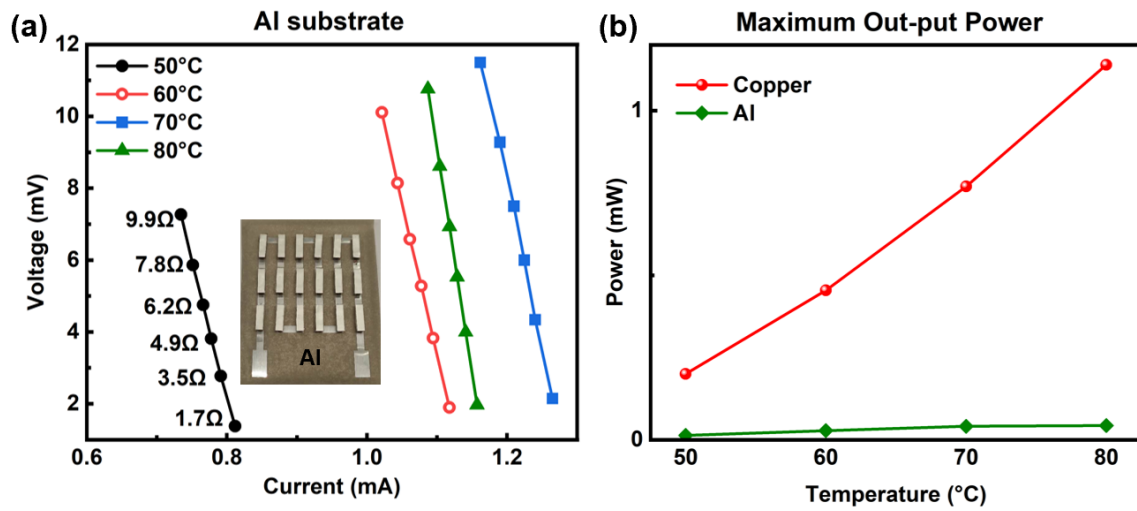
Figure 23: (a) I-V curve of Al substrate device (b) Maximum output power comparison

aluminium oxide and prevent its formation. Even though the output power of Al substrate devices is exceedingly lower than the conventional device, it still gives a guideline for low-cost FTEMs. The balance between the cost and output power can be manipulated to maximize the total profit. What's more, it is worth noticing that the maximum output power is around half of the ATOM907 based device with a copper substrate. Hence, it is still significant to use Al-PET as substrate materials.

5 Summary and outlook

In conclusion, I studied the performance of 2D-ECA as a binding material in FTEMs and compared its performance with two types of both solder pastes and commercial ECAs in this work. The result shows that the mechanical strength of 2D-ECA is superior to part of the commercial binding materials and as high as the best commercial products. However, the electrical resistance of 2D-ECA is excessively high due to the contact resistance, especially compared to solder paste. That arises from the different principles in forming a joint. Nevertheless, the resistance of 2D-ECA is lower than the commercial ATOM917. Further comparison in output power indicates that internal resistance is the key factor that influences the thermoelectric property of FTEMs. Since the internal resistance of 2D-ECA based device is considerably higher than the solder paste, the output power is also lower than the solder paste. Thus, further research is still required to reduce the contact resistance between 2D-ECA and metal substrates. Nevertheless, 2D-ECA can be fabricated on Al-coated PET substrates, which is relatively cheaper than conventional Cu-coated PI substrates, indicating a promising trend in reducing the cost of FTEMs. Compared to 2D-ECA, solder pastes can not work on Al substrates.

Additionally, the fabrication method in my thesis work relies too much on hand work, especially in the design of flexible devices, which is obviously not suitable for repeating the experiment or industrial production. One possible way is to put the full-size substrate that has been printed with binding materials on top of the pellets and use the laser machine to remove the edge substrates, leaving the layer with copper. It is also a feasible method to manufacture a flexible device. What's more, the devices can also be filled with flexible low thermal electric materials. On the one hand, the materials can protect the device from external force. On the other hand, it will also increase the temperature gradient according to Fourier's law of heat conduction. These are possible approaches towards superior FTEMs.

References

[1]   https://www.ecotricity.co.uk/our-green-energy/energy-independence/the-end-of-fossil-fuels.

[2]   https://commons.wikimedia.org/w/index.php?curid=3372874.

[3]   https://ph.rs-online.com/web/p/peltier-modules/4901351.

[4]   https://www.pveducation.org/pvcdrom/characterisation/four-point-probe-resistivity-measurements.

[5]   Robert D Adams. *Adhesive bonding: science, technology and applications.* Woodhead Publishing, 2021.

[6]   MR Adibeig et al. "Experimental and numerical study of polyethylene hybrid joints: friction stir spot welded joints reinforced with adhesive". In: *International Journal of Adhesion and Adhesives* 98 (2020), p. 102555.

[7]   Pietro P Altermatt et al. "Reassessment of the intrinsic carrier density in crystalline silicon in view of band-gap narrowing". In: *Journal of Applied Physics* 93.3 (2003), pp. 1598–1604.

[8]   Neil W Ashcroft and N David Mermin. *Solid state physics.* Cengage Learning, 2022.

[9]   D Baluch and G Minogue. "Fundamentals of solder paste technology". In: *Global SMT & Packaging* (2007).

[10] Dan Bousfield. "Revisiting cyber-diplomacy: Canada–China relations online". In: *Globalizations* 14.6 (2017), pp. 1045–1059.

[11] Olga Bubnova. "Thermoelectric properties of conducting polymers". PhD thesis. Linköping University Electronic Press, 2013.

[12] Duck-Young Chung et al. "CsBi4Te6: A high-performance thermoelectric material for low-temperature applications". In: *Science* 287.5455 (2000), pp. 1024–1027.

[13] Joseph R Davis. *Tensile testing.* ASM international, 2004.

[14] Shuo Deng et al. "Enhanced thermoelectric performance of twisted bilayer graphene nanoribbons junction". In: *Carbon* 145 (2019), pp. 622–628.

[15] Yoomin Eom et al. "Flexible thermoelectric power generation system based on rigid inorganic bulk materials". In: *Applied energy* 206 (2017), pp. 649–656.

[16] Jiaqing He et al. "On the origin of increased phonon scattering in nanostructured PbTe based thermoelectric materials". In: *Journal of the American Chemical Society* 132.25 (2010), pp. 8669–8675.

[17] Sile Hu et al. "Metal Halide Perovskites as Emerging Thermoelectric Materials". In: *ACS Energy Letters* 6.11 (2021), pp. 3882–3905.

[18] Yadali Jamaloei et al. "The Joule-Thomson Effect in Petroleum Fields: I. Well Testing, Multilateral/Slanted Wells, Hydrate Formation, and Drilling/Completion/Production Operations". In: *Energy Sources, Part A: Recovery, Utilization, and Environmental Effects* 37.2 (2015), pp. 217–224.

[19] Deep Jariwala et al. "Carbon nanomaterials for electronics, optoelectronics, photovoltaics, and sensing". In: *Chemical Society Reviews* 42.7 (2013), pp. 2824–2860.

[20] Nesrine Jaziri et al. "A comprehensive review of Thermoelectric Generators: Technologies and common applications". In: *Energy Reports* 6 (2020), pp. 264–287.

[21] Kyung Kuk Jung et al. "Flexible thermoelectric generator with polydimethyl siloxane in thermoelectric material and substrate". In: *Current Applied Physics* 16.10 (2016), pp. 1442–1448.

[22] Choong Sun Kim et al. "Self-powered wearable electrocardiography using a wearable thermoelectric power generator". In: *ACS Energy Letters* 3.3 (2018), pp. 501–507.

[23] Sun Jin Kim, Ju Hyung We, and Byung Jin Cho. "A wearable thermoelectric generator fabricated on a glass fabric". In: *Energy & Environmental Science* 7.6 (2014), pp. 1959–1965.

[24] Nianling Kuang et al. "High performance flexible thermoelectric generator using bulk legs and integrated electrodes for human energy harvesting". In: *Energy Conversion and Management* 272 (2022), p. 116337.

[25] Giovanni Leonida. *Handbook of printed circuit design, manufacture, components & assembly.* Electrochem. Publ., 1981.

[26] Wenjie Li et al. "Conformal High-Power-Density Half-Heusler Thermoelectric Modules: A Pathway toward Practical Power Generators". In: *ACS Applied Materials & Interfaces* 13.45 (2021), pp. 53935–53944.

[27] Johan Liu et al. "Overview of conductive adhesive joining technology in electronics packaging applications". In: *Proceedings of 3rd International Conference on Adhesive Joining and Coating Technology in Electronics Manufacturing 1998 (Cat. No. 98EX180).* IEEE. 1998, pp. 1–18.

[28] Zhisong Lu et al. "Silk fabric-based wearable thermoelectric generator for energy harvesting from the human body". In: *Applied energy* 164 (2016), pp. 57–63.

[29] Deepa Madan et al. "Printed flexible thermoelectric generators for use on low levels of waste heat". In: *Applied energy* 156 (2015), pp. 587–592.

[30] Cristina V Manzano et al. "Anisotropic effects on the thermoelectric properties of highly oriented electrodeposited Bi2Te3 films". In: *Scientific reports* 6.1 (2016), p. 19129.

[31] Saeed Masoumi, Seamus O'Shaughnessy, and Amir Pakdel. "Organic-based flexible thermoelectric generators: From materials to devices". In: *Nano Energy* 92 (2022), p. 106774.

[32] Irfan Mir and D Kumar. "Recent advances in isotropic conductive adhesives for electronics packaging applications". In: *International journal of adhesion and adhesives* 28.7 (2008), pp. 362–371.

[33] Robert J Moffat. "Notes on using thermocouples". In: *Electronics Cooling* 3 (1997), pp. 12–15.

[34] Rafiq Mulla, Daniel R Jones, and Charles W Dunnill. "Thermoelectric paper: graphite pencil traces on paper to fabricate a thermoelectric generator". In: *Advanced Materials Technologies* 5.7 (2020), p. 2000227.

[35] Lars Onsager. "Reciprocal relations in irreversible processes. I." In: *Physical review* 37.4 (1931), p. 405.

[36] Jean Charles Athanase Peltier. *Nouvelles expériences sur la caloricité des courans électriques.* 1834.

[37] Daniel D Pollock. *Thermoelectricity: theory, thermometry, tool.* 852. ASTM International, 1985.

[38] G Joseph Poon. "Electronic and thermoelectric properties of half-Heusler alloys". In: *Semiconductors and semimetals.* Vol. 70. Elsevier, 2001, pp. 37–75.

[39] David Michael Rowe. *Materials, preparation, and characterization in thermoelectrics.* CRC press, 2017.

[40] David Michael Rowe. *Thermoelectrics handbook: macro to nano.* CRC press, 2018.

[41] B Sherman, Robert R Heikes, and Roland W Ure Jr. "Calculation of efficiency of thermoelectric devices". In: *Journal of Applied Physics* 31.1 (1960), pp. 1–16.

[42] Masahiro Shikano and Ryoji Funahashi. "Electrical and thermal properties of single-crystalline (Ca 2 CoO 3) 0.7 CoO 2 with a Ca 3 Co 4 O 9 structure". In: *Applied physics letters* 82.12 (2003), pp. 1851–1853.

[43] G Jeffrey Snyder and Eric S Toberer. "Complex thermoelectric materials". In: *Nature materials* 7.2 (2008), pp. 105–114.

[44] JE Sohn and U Ray. "Weak organic acids and surface insulation resistance". In: *Circuit World* (1995).

[45] Xiaoqin Sun et al. "Experimental research of a thermoelectric cooling system integrated with gravity assistant heat pipe for cooling electronic devices". In: *Energy Procedia* 105 (2017), pp. 4909–4914.

[46] Karol Sztekler et al. "The thermoelectric generators use for waste heat utilization from cement plant". In: *E3S Web of Conferences.* Vol. 14. EDP Sciences. 2017, p. 01031.

[47] William Thomson. "4. on a mechanical theory of thermo-electric currents". In: *Proceedings of the Royal society of Edinburgh* 3 (1857), pp. 91–98.

[48] MV Vedernikov and EK Iordanishvili. "AF Ioffe and origin of modern semiconductor thermoelectric energy conversion". In: *Seventeenth International Conference on Thermoelectrics. Proceedings ICT98 (Cat. No. 98TH8365).* IEEE. 1998, pp. 37–42.

[49] Yancheng Wang et al. "Wearable thermoelectric generator to harvest body heat for powering a miniaturized accelerometer". In: *Applied energy* 215 (2018), pp. 690–698.

[50] Frank Wenner. *A method of measuring earth resistivity.* 258. US Government Printing Office, 1916.

[51] Xiaomin Xu et al. "Poly (N-isopropylacrylamide)-based thermoresponsive composite hydrogels for biomedical applications". In: *Polymers* 12.3 (2020), p. 580.

[52] Byung-Seung Yim et al. "Characteristics of solderable electrically conductive adhesives (ECAs) for electronic packaging". In: *Microelectronics Reliability* 52.6 (2012), pp. 1165–1173.

[53] Byung-Seung Yim et al. "Self-interconnection characteristics of hybrid composite with low-melting-point alloy fillers". In: *Journal of composite materials* 47.9 (2013), pp. 1141–1152.

[54] HS Yoder Jr. "Timetable of petrology". In: *Journal of Geological Education* 41.5 (1993), pp. 447–489.

[55] FG Yost, FM Hosking, and DR Frear. "Introduction: The Mechanics of Solder alloy wetting and spreading". In: *The Mechanics of solder alloy wetting and spreading.* Springer, 1993, pp. 1–7.

[56] Xiaoliang Zeng et al. "Silver telluride nanowire assembly for high-performance flexible thermoelectric film and its application in self-powered temperature sensor". In: *Advanced Electronic Materials* 5.2 (2019), p. 1800612.

[57] Xuan Zhao et al. "Fabrication of transparent paper-based flexible thermoelectric generator for wearable energy harvester using modified distributor printing technology". In: *ACS applied materials & interfaces* 11.10 (2019), pp. 10301–10309.
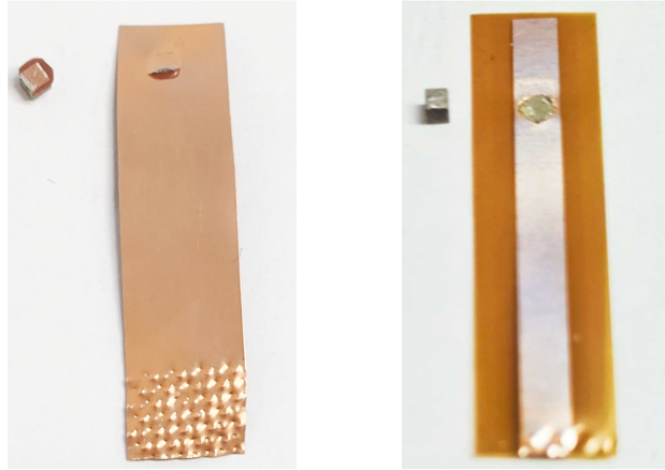
A   Appendix

Figure A1: Breaking results of 2D-ECA based sample (left) and OM550 solder paste based sample (right)
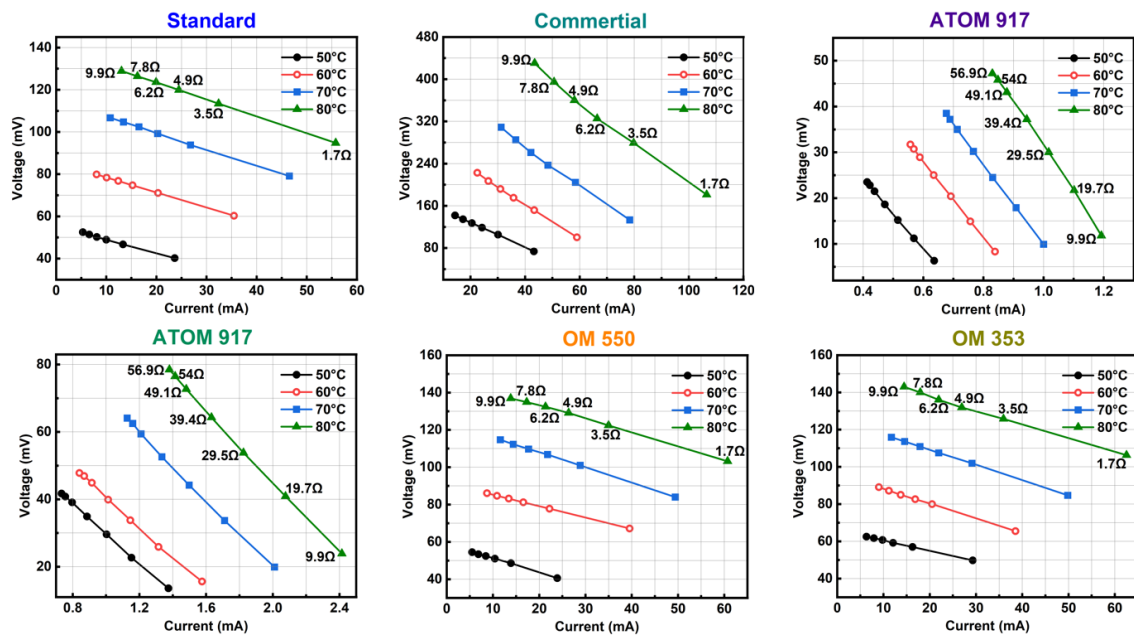

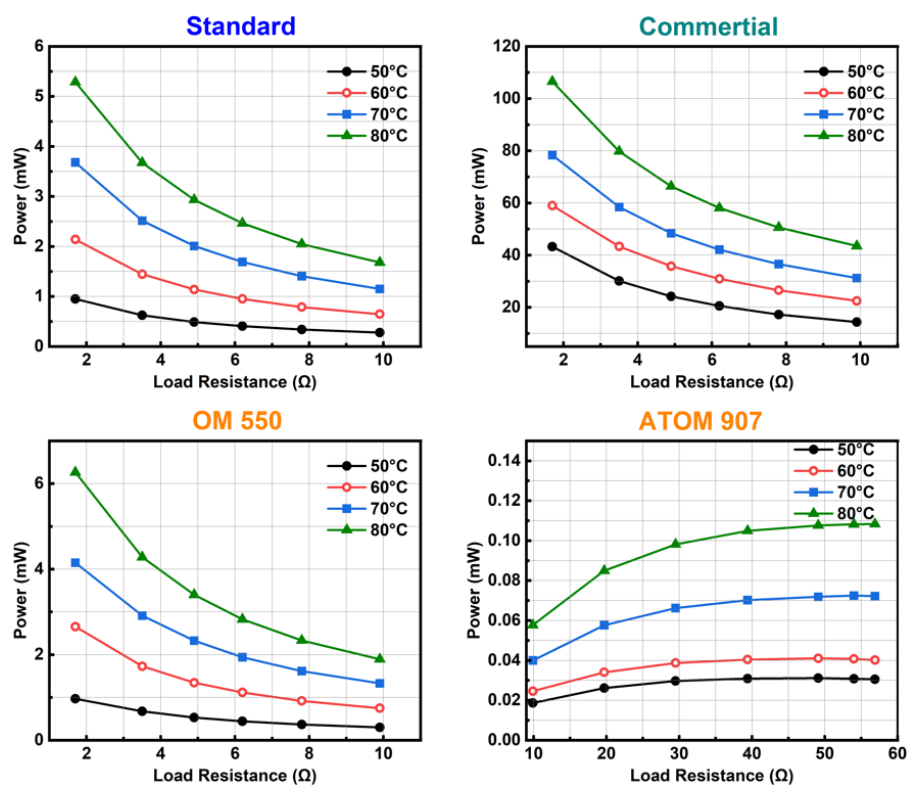Figure A2: I-V curves of different materials based modules

Figure A3: Maximum output power of different materials based modules